

THE GAS DISTRIBUTION IN THE CENTRAL REGION OF THE GALAXY. II. CARBON MONOXIDE

H. S. LISZT AND W. B. BURTON

National Radio Astronomy Observatory,* Green Bank, West Virginia

Received 1978 May 4; accepted 1978 June 7

ABSTRACT

The kinematic arrangement of 2.6 mm CO emission from the inner ~ 3 kpc of the Galaxy is essentially identical to that of atomic hydrogen. Molecular emission from the inner Galaxy is strongly present 3° – 10° from the galactic nucleus at $b \neq 0^\circ$ and clearly is tilted in the manner predicted by the model of the inner Galaxy described in the first paper of this series. The geometry and kinematics of that model also dominate the smaller-scale behavior of high-velocity CO emission observed closer to $l = 0^\circ$.

Synthetic CO line profiles generated in accord with the tilted-disk model of the inner Galaxy reproduce the prominent “expanding molecular ring” and “ 165 km s^{-1} ” feature observed in the galactic equator around $l \approx 0^\circ$. These features are consequences of the transformation of emission from gas in the rotating and expanding tilted disk into the observed quantities; neither kinematic nor density perturbations are necessarily implied by their existence. We argue that differences in appearance between the H I and the CO material result from the low contrast available in CO mapping and from comparison of optically thick and thin emission lines.

The CO/H I intensity ratio is anomalously large in the inner Galaxy. Molecular gas is overabundant relative to the rest of the Galaxy. We estimate the mass of the molecular component of the inner-Galaxy disk $M_{\text{H}_2} \gtrsim 10^9 M_\odot$ and the mean molecular density $\langle n_{\text{H}_2} \rangle \gtrsim 25 \text{ cm}^{-3}$. Even at the lowest densities compatible with the observations, the inner Galaxy contains enough gas in molecular form to fill the region between $0 \leq \varpi \leq 4$ kpc at a mean density $\langle n_{\text{H}_2} \rangle \approx 3 \text{ cm}^{-3}$.

Subject headings: galaxies: Milky Way — galaxies: nuclei — galaxies: structure —
 interstellar: matter — interstellar: molecules

I. INTRODUCTION

Observations of molecular spectra in the direction of the inner Galaxy have revealed a variety of features which are commonly described as peculiar to molecular kinematics and not shared by the neutral but atomic gas sampled at 21 cm. The most prominent example of a “uniquely” molecular feature is the “expanding molecular ring” crossing $l = 0^\circ$ at $v = -135 \text{ km s}^{-1}$ and dominating the absorption spectra of OH and H_2CO (see, e.g., Scoville 1972; Kaifu, Kato, and Iguchi 1972; Cohen and Few 1976). Although the positive-velocity part of the original ring model is not in evidence, Oort (1977) has speculated that the “ 165 km s^{-1} expanding feature” of Sanders and Wrixon (1974) might complete a symmetric structure which could be attributed to a single expulsive event. Bania’s (1977) extensive discussion of models for the molecular ring also treats the positive- and negative-velocity features as parts of a single entity. Although Sanders, Wrixon, and Mebold (1977) have recently demonstrated that the positive-velocity feature has a counterpart in H I, the molecular ring model has not entered the interpretation of the

extensive 21 cm data. Conversely, the “rotating nuclear disk” model of the H I distribution introduced by Rougoor and Oort (1960) has not been used widely in the context of molecular observations. A pronounced pure-rotation signature, while present in a portion of the molecular gas (Liszt *et al.* 1977), does not dominate molecular spectra.

The molecular ring and other anomalous features have been interpreted and analyzed in terms of a variety of mechanisms. These include anisotropic ejecta (see the review by Oort 1977), isotropic explosions (Sanders and Bania 1976), dispersion phenomena (Bania 1977), and a spiral pattern extending close to the galactic center (Scoville, Solomon, and Jefferts 1974). Such analyses usually imply that the observed molecular spectral features have their origins in locatable material bodies or in kinematic perturbations which are largely peculiar to the molecular gas (the model of Scoville *et al.* is an exception). Particular problems for models postulating violent nuclear activity include the essentially complete azimuthal symmetry of the molecular ring, and the fundamental problem of the high abundance of molecular species which require quiescent conditions for their very existence.

Here we present new observations of CO in the inner Galaxy, together with a new interpretation of the expanding molecular features and of the more

† Operated by Associated Universities, Inc., under contract with the National Science Foundation.

general distribution and kinematics of carbon monoxide emission in the inner ~ 3 kpc of the Galaxy. The context in which the observations are interpreted is the tilted-disk model of the inner Galaxy described by Burton and Liszt (1978, Paper I). This model accounts for a variety of H I spectral features previously thought to be noninterrelated; examples of these include the “connecting arm” of Rougoor (1964), the “rotating nuclear disk,” and many seemingly isolated “ejecta.” The tilted-disk model is summarized in § II. In § III we describe the new carbon monoxide observations against which the model is tested. In § IV we show that the molecular ring and other features of the observations are reproduced by the same model which accounts for H I emission, as artifacts of transforming the emission from the smoothly distributed molecular gas in the tilted disk into the observed coordinates and intensities. Also in § IV we compare the longitude-velocity arrangements of H I and CO away from the plane $b = 0^\circ$. This comparison illustrates the presence of the model signature in the molecular observations extending as far as $l \approx 9^\circ$, and indicates that the atomic gas and molecular gas have similar distributions and motions. This comparison also allows us to argue that the differences in *appearance* between 21 cm and 2.6 mm emission arise naturally as the result of signal-to-noise considerations and of the different nature of the radiation transport in the two lines. In § V we illustrate the latitude-velocity arrange-

ment of molecular emission near the plane $b = 0^\circ$. These observations directly show the tilts of the inner-Galaxy gas distribution and demonstrate the regularity of molecular kinematics on smaller angular scales than are accessible at longer wavelengths. In § VI we consider the physical properties of the molecular gas in the inner Galaxy. The principal results contained in the paper are summarized in § VII.

II. THE TILTED-DISK MODEL

The tilted-disk model of the inner Galaxy and the bulk of the (H I) observations used to define it are discussed in Paper I. We summarize it briefly here. The model constrains the inner-Galaxy gas distribution to a disk of radius $\varpi_d' = 1.5$ kpc whose orientation is described by the position angle $\alpha = 22^\circ$ and inclination angle $i = 78^\circ$. The angle α is measured counterclockwise in the plane of the sky; $\alpha > 0^\circ$ implies that the disk will appear mainly where l and b are of opposite sign. The inclination angle has its usual meaning such that $i = 0^\circ$ and $i = 90^\circ$ represent, respectively, face-on and edge-on viewing of the disk. The angle between the disk axis and that of the Galaxy at large is $\cos^{-1}(\cos \alpha \sin i) \approx 25^\circ$; the apparent major axis of the midplane of the disk coincides approximately with the locus $b = -l \tan \alpha$. A projection of the disk onto observational galactic coordinates is shown in Figure 1. The dashed loci are projections of the boundaries of a cylinder extending

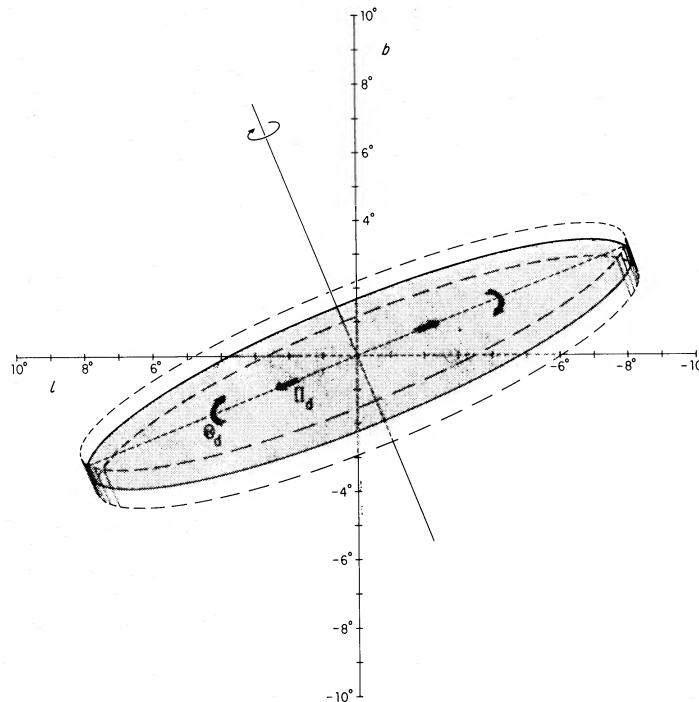


FIG. 1.—Appearance of the model tilted gas distribution as projected onto the plane of the sky in angular coordinates. The solid-line approximate ellipse represents the equatorial plane, where $z_d = 0$ pc, of a disk of radius $\varpi_d = 1.5$ kpc tilted through the angles discussed in the text: $\alpha = 22^\circ$, $i = 78^\circ$. The dashed lines correspond to disks at heights $z_d = \pm 100$ pc. The vectors indicate schematically the rotation parameter $\Theta_d(\varpi_d)$ and the expansion parameter $\Pi_d(\varpi_d)$.

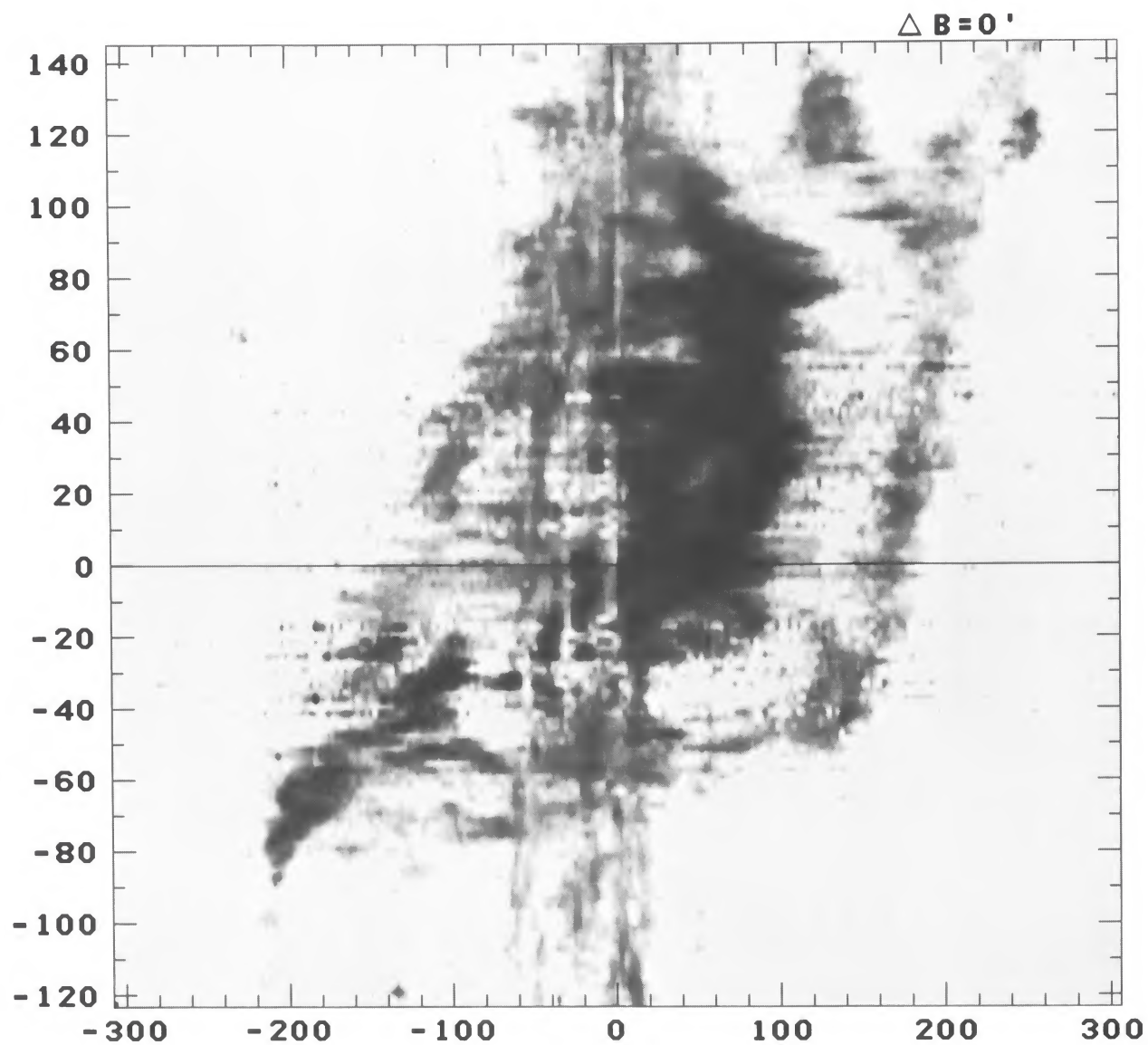


FIG. 2*b*.—Gray-scale representation of the longitude-velocity arrangement of CO emission at $\Delta b = 0'$ ($b = -3'$), as in Fig. 2*a*.

± 0.1 kpc from the mean plane $z_d = 0$ pc. Density within the model varies only with z_d , in a Gaussian manner with dispersion 0.1 kpc. Note that Figure 1 contains a variety of projection effects caused by the appreciable size of the disk, 3 kpc, compared to the Sun-center distance, here taken as $\varpi_0 = 10$ kpc. For example, the nearer portions of the disk at $l > 0^\circ$, $b < 0^\circ$ subtend a noticeably larger solid angle than the more distant regions. A more complete discussion of such behavior appears in Paper I, as similar effects are actually present in the more complete data on the larger-scale H I distribution.

Within the disk, expansion and rotation motions are of comparable magnitude. The functional form of the expansion is

$$\Pi_d(\varpi_d) = 170[1 - \exp(-\varpi_d/0.07)] \text{ km s}^{-1}, \quad (1)$$

with ϖ_d , the perpendicular distance from the disk axis, expressed in kpc. The rotation motion is symmetrical with respect to $\varpi_d = 0.85$ kpc:

$$\begin{aligned} \Theta_d(\varpi_d) &= 180[1 - \exp(-\varpi_d/0.20)] \text{ km s}^{-1} \\ &(\varpi_d \leq 0.85 \text{ kpc}) \\ &= 180\{1 - \exp[-(1.7\varpi_d)/0.20]\} \text{ km s}^{-1} \\ &(\varpi_d > 0.85 \text{ kpc}). \end{aligned} \quad (2)$$

These functions are illustrated in Paper I and are compared there with previously derived rotation curves for inner-Galaxy material. Recognition of the pervasive nature of the expansion component in the gas in the inner-Galaxy disk implies a rotation component smaller in magnitude and increasing less rapidly with distance near the galactic center than what results if expansion is not considered a morphological property of the kinematics (cf. Sanders and Lowinger 1972; Oort 1977). Specification of the rotation component in Paper I principally involved fitting observed and modeled terminal velocities for H I along the line of greatest kinematic symmetry $b = -l \tan \alpha$: this procedure involves some iteration but is quite straightforward once Π_d is specified. Note that the expansion is essentially constant and that the rotation motions are specified along only a single line. Only when the gas motions have extremely regular and axially symmetric behavior is such a procedure likely to produce a good fit to observations taken far from the apparent major axis of the model.

The expansion function is most directly seen in the direction $l = 0^\circ$, where rotation is predominantly transverse to the line of sight. The magnitude of the radial velocity in this direction follows directly from the extreme velocities; the presence of absorption against the nuclear continuum sources in H I, OH, and H₂CO at negative velocities shows that the direction of the radial motion is outward. The velocities in profiles measured in directions increasingly removed from the direction of the axis of the disk are increasingly dominated by the rotation component of the disk. The CO observations provide much higher angular resolution than that provided

by the H I data and consequently provide more information on the velocity field measured in directions close to that of the rotation axis. In addition, the CO data are less contaminated than the H I data by absorption against the nuclear sources, and contain less confusion from the foreground and background contributions from the Galaxy at large.

The line-of-sight velocity of a point within the disk at a distance r (kpc) from the Sun is

$$\begin{aligned} v_d &= \Pi_d(\varpi_d)[\varpi_d^2 - \varpi_0(\varpi_0 - r \cos b \cos l - z_d \cos i)] \\ &\times (\varpi_d r)^{-1} - \Theta_d(\varpi_d)\varpi_0 \sin i \\ &\times (\sin b \sin \alpha - \cos b \sin l \cos \alpha)/\varpi_d \\ &- \Theta_0 \sin l \cos b. \end{aligned} \quad (3)$$

At the Sun's location we use $\varpi_0 = 10$ kpc and $\Theta_0 = 250$ km s⁻¹. The synthetic CO profiles in this paper follow from solving the radiative transfer equation assuming LTE and incorporating the disk velocity field.

In Paper I the physical properties of the H I were taken over essentially unchanged from model fits to gas in the Galaxy at large, i.e., $T_{\text{spin}} = 120$ K, $n_{\text{H}} = 0.33$ cm⁻³, and internal dispersion $\sigma = 9$ km s⁻¹. The physical properties of the molecular gas throughout the Galaxy are less well understood, and, as we discuss in § VI, it is likely that the inner-Galaxy molecular constituent has properties unique in several regards. To model the carbon monoxide emission, we took as a constraint the typically observed intensities 2–4 K, which imply that the excitation temperature of the $J = 1-0$ transition $T_{\text{ex}} \gtrsim 6-8$ K. Excitation of this order, if done by collisions alone, requires simply that the gas pressure $n_{\text{H}_2} T_k$ satisfy the condition $n_{\text{H}_2} T_k \gtrsim 1-2 \times 10^4$ cm⁻³ K if the kinetic temperature $T_k \gtrsim 15$ K (see the discussion in § VI). For the purposes of constructing synthetic emission profiles, we took $T_k = 120$ K, $n_{\text{H}_2} = 150$ cm⁻³, $\sigma = 9$ km s⁻¹, and a fractional abundance $[\text{CO}]/[\text{H}_2] = 6 \times 10^{-5}$.

III. OBSERVATIONAL MATERIAL

The CO observations discussed here were taken in observing periods from 1975 May to 1978 January, at the NRAO 36 foot (11 m) telescope on Kitt Peak. Their properties are similar to those presented by Liszt *et al.* (1977) and need not be repeated at length here. The velocity resolution of the spectra presented below is 5 km s⁻¹. The half-power beamwidth of the telescope at 2.6 mm is 1'; however, the angular resolution of the present data is set by the spacing between observations, which is mentioned for each position-velocity map in the appropriate figure legend. Intensities are given in terms of the corrected antenna temperature T_A^* divided by a nominal value of the beam efficiency $\eta = 0.65$. For an isothermal cloud which uniformly fills only the main beam of the telescope with material at excitation temperature T_{ex} ,

$$\begin{aligned} T_A^*/\eta &= 5.51[1 - \exp(-\tau)] \\ &\times \{[\exp(5.51/T_{\text{ex}}) - 1]^{-1} - 0.162\} \text{ K}, \end{aligned} \quad (4)$$

where the factor 0.162 represents the blackbody background at 2.8 K.

The measured radial velocities in this paper are referred to the local standard of rest. Positions are given both in terms of the usual galactic coordinates (l, b) and in terms of displacements from the $2\ \mu\text{m}$ radiation peak in Sgr A West ($\Delta l, \Delta b$). The coordinates of this peak are $l = -3.3$, $b = -2.8$ (Becklin and Neugebauer 1975).

IV. THE LONGITUDE-VELOCITY ARRANGEMENT OF THE INNER-GALAXY CO EMISSION

a) Observations in the Galactic Equator; the "Molecular Ring"

Investigations of the molecular emission from the inner Galaxy have concentrated exclusively on regions close to the plane $b = 0^\circ$ (e.g., Scoville *et al.*; Liszt *et al.* 1977; Bania 1977). This restriction, necessitated by the small amount of observing time available, is unfortunate in view of the picture of the inner-Galaxy gas distribution which we defend here. It is clear that, if the gas is distributed as suggested by Figure 1, a single l - v cut at $b = 0^\circ$ will represent only certain limited aspects of the distribution.

Figure 2a shows contours of carbon monoxide emission intensity in l - v coordinates between $l = -123'$ and $l = 145'$ at the latitude $b = -3'$, $\Delta b = 0'$, of Sgr A West. The contour levels represent $T_A^* = 1.3, 3, 5, 7.5, 11, 15, 20, 25, \dots$ K. Figure 2b shows the same data in a more readily accessible, but less quantitative, gray-scale representation. (Fig. 1b of Liszt *et al.* 1977 is a useful schematic rendering of an earlier, less extensive sample of the observations at $\Delta b = 0'$.) The emission counterpart of the "expanding molecular ring" extends at least over the range $-50' < l < 90'$, crossing $l = 0'$ at $v = -135\ \text{km s}^{-1}$: at $l \approx -50'$ it could either cross over to positive velocities or continue on at $v \approx -200\ \text{km s}^{-1}$. High-velocity emission (the $165\ \text{km s}^{-1}$ expanding feature near $l = 0'$) has a dissimilar longitude extent, from $l = -50$ to $l > 145'$, and exhibits no tendency to join with emission from the ring at positive longitudes. Even if one identifies the high-velocity gas with the front and back halves of a symmetrical structure in the plane $b = 0'$, the observations are not obviously compatible with the oval-shaped locus in the l - v plane which would be occupied by such a body.

Figure 3 shows intensity contours in l - v coordinates which correspond to synthetic profiles produced when the Figure 1 disk distribution is sampled with a line beam at $2'$ intervals of longitude. Discrete spectral features appear as consequences of velocity crowding alone, despite smooth variation of the disk's physical parameters and despite the axisymmetric disk kinematics. Near $l = 0'$, Θ_d velocities are nearly transverse to the line of sight, with nearly all emission consequently projected onto two narrow velocity ranges specified by $\pm \Pi_d$.

The model profiles reproduce most of the observational characteristics of the high-velocity gas. The most important of these are the existence of distinct

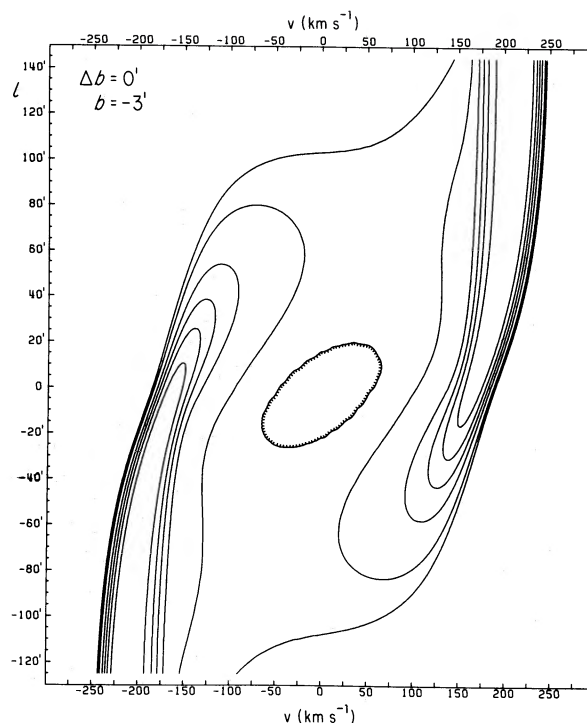


FIG. 3.—Synthetic longitude-velocity diagram of CO emission at $\Delta b = 0'$ ($b = -3'$) generated by the model gas distribution illustrated in Fig. 1 and discussed in the text. The discrete spectral features resembling the molecular ring and $165\ \text{km s}^{-1}$ expanding feature are produced solely by velocity crowding. They cross the plane $l \approx 0'$ with nearly equal $|v|$. As discussed in the text, the positive average velocity of the two observed molecular features may indicate that the kinematic center of the inner-Galaxy distribution lies at negative longitudes.

positive- and negative-velocity emission branches, the differing longitude extents of these branches, and their dissimilar dv/dl slopes. The model accounts for the difference in the slopes, which is seen prominently in comparing the two branches as they are observed at positive longitudes. In view of the similarities between the observed molecular ring signature and the synthesized pattern following from the predictions of the tilted-disk model, we conclude that the "molecular ring" does not correspond to a discrete feature in space but rather is the natural consequence of the transformation into the observed coordinates of emission from gas smoothly distributed in the tilted disk defining the gas distribution in the central region of the Galaxy. This conclusion is supported in the following sections by arguments that the CO distribution is similar to the H I distribution—which justifies interpreting the CO data in terms of a model based in the first instance on the more extensive H I data—and by additional direct evidence in the CO material for the validity of the tilted-disk distribution.

b) Observations Away from the Galactic Equator

Although the CO emission is concentrated to $-2^\circ \lesssim l \lesssim 2^\circ$ at $b = 0^\circ$, the tilts in the model (which

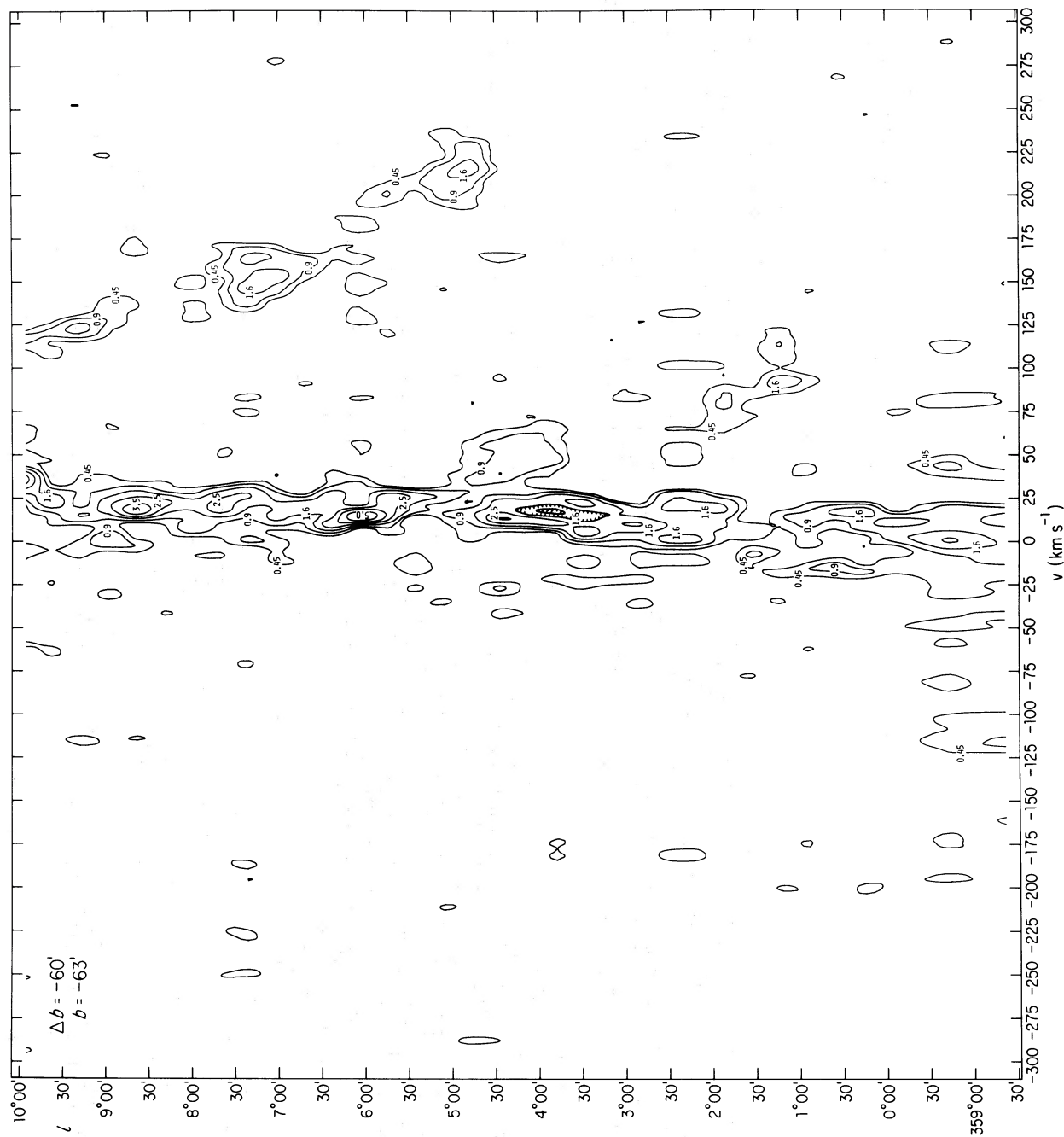


Fig. 4a.—Longitude-velocity arrangement of CO emission at $\Delta b = -60'$ as observed with $20'$ beam spacings and 5 km s^{-1} velocity resolution. The emission at $4^\circ \lesssim l \lesssim 10^\circ$, $100 \text{ km s}^{-1} \lesssim v \lesssim 225 \text{ km s}^{-1}$ is the "connecting arm" of Rougoor (1964) seen in H I in Fig. 5.

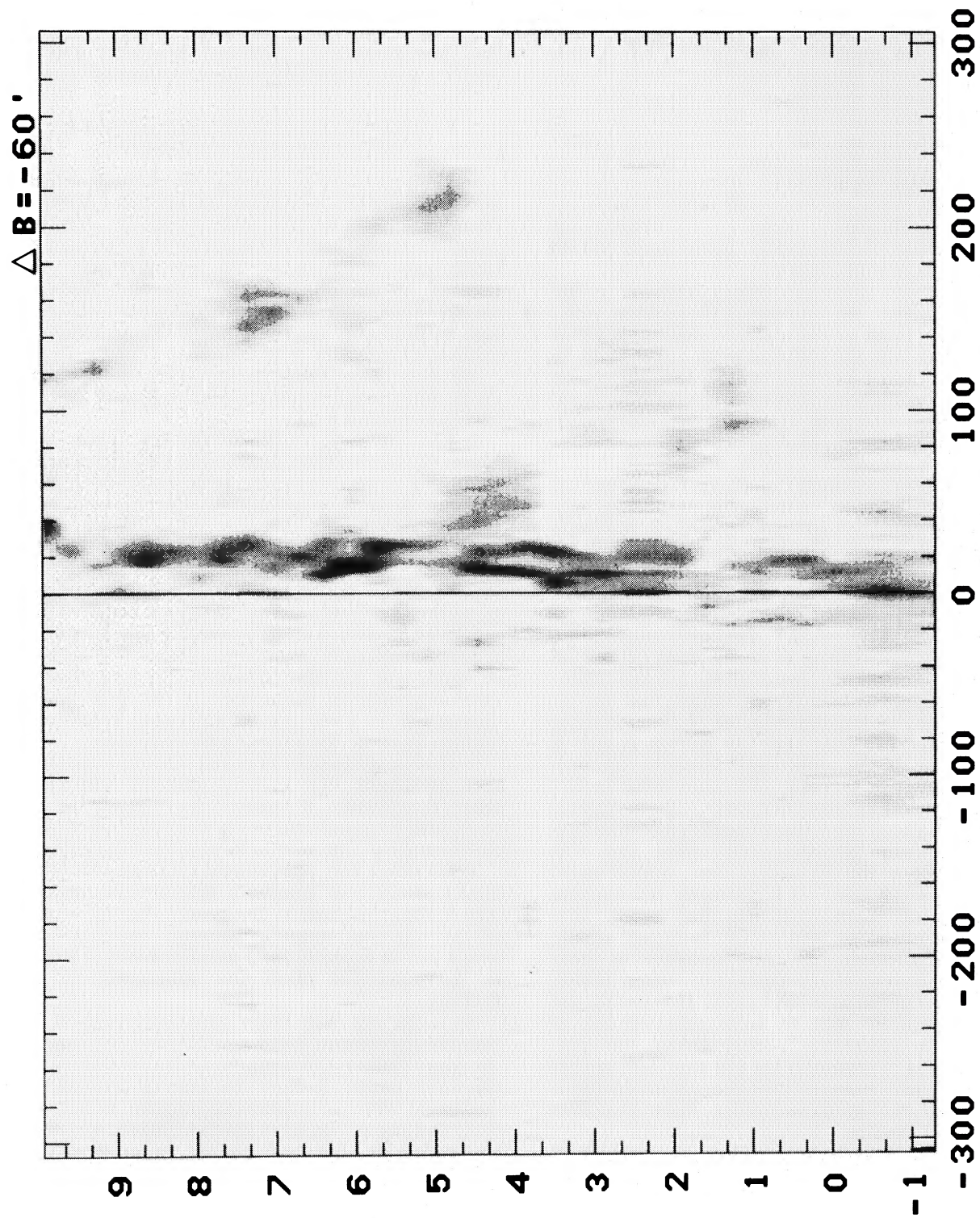


FIG. 4b.—Gray-scale representation of the longitude-velocity arrangement of CO emission at $\Delta b = -60'$, as in Fig. 4a

are derived rather directly from H I moment maps in Paper I) imply that the longitude and velocity ranges which predominate should vary as the latitude of observation is varied. Figure 1 can give a qualitative indication of the predicted variations. At $b > 0^\circ$ the tilted-disk contribution should dominate at $l < 0^\circ$. At $b < 0^\circ$ the situation is reversed. Considering an l - v cut at $b = +1^\circ$, one can see from Figure 1 that, near $l = 0^\circ$, the expansion and rotation terms both contribute positive-velocity emission; the emission will continue to be concentrated at positive velocities as l decreases until, at some negative longitude, the line-of-sight components of Θ_a and Π_a cancel, resulting in emission near $v \approx 0 \text{ km s}^{-1}$. At $b = -1^\circ$ one expects more emission from $l > 0^\circ$ than from $l < 0^\circ$; one expects a positive-velocity component from Θ_a to dominate at sufficiently large $l > 0^\circ$, whereas at lower longitudes the Θ_a and Π_a components will be of opposite sign until $l \approx 1^\circ$.

To investigate these predictions inherent in the tilted-disk model, we observed CO at $\Delta b = \pm 60'$. The emission in an l - v cut at $\Delta b = -60'$ is shown in Figures 4a and 4b; the emission in an l - v cut at $\Delta b = +60'$ is shown in Figures 6a and 6b. In addition, we include for comparison with the CO distribution the H I data at $b = -60'$ (Fig. 5) and at $b = +60'$ (Fig. 7). The H I maps are comprised of material described in Paper I.

At $\Delta b = -60'$ the dominant H I feature associated with the galactic-center region is the positive-velocity "connecting arm" of Rougoor (1964). It has been interpreted variously as a bar, spiral arm, and expanding arc by, respectively, Kerr (1967), van der Kruit (1970), and Cohen and Davies (1976). In Paper I we show that this feature of the H I observations is a natural consequence of the tilted-disk distribution and that its contrary locus in the l - v plane reflects the decrease in the rotation speed at $\varpi_a \gtrsim 1 \text{ kpc}$. Comparison of Figure 4a with Figure 5 shows that the CO emission pattern coincides with the H I "connecting arm" feature. Evidently this CO pattern is also a manifestation of the tilted disk. Much of the disk signature at $l < 3^\circ$ in Figure 5 is quite weak in H I and simply below our detection limit ($\sim 0.4 \text{ K}$) in CO.

Figures 6 and 7 show the comparable l - v arrangement of emission at $\Delta b = +60'$. Here also, CO emission follows the H I ridge lines, appearing at intensities greater than $\sim 1 \text{ K}$ whenever the antenna temperature at 21 cm is greater than $\sim 5 \text{ K}$. The positive-velocity ridge seen in CO is typical of the sort of features which are usually considered as ejecta from the nucleus at 21 cm. Because of contamination from the general galactic layer in the H I spectra, the pattern cannot be seen to cross zero velocity at $l \approx -5^\circ$, $v = -210 \text{ km s}^{-1}$. Nonetheless, this predicted crossing is present in the CO data with typical intensities, which indicates that the gas producing it is similar to that producing other, more obviously extended H I features.

Thus molecular features intimately associated with the inner-Galaxy distribution may be followed to distances $\sim 1.5 \text{ kpc}$ from Sgr A. Emission patterns

which appear in the H I material appear in the CO data with intensities which approximately follow the ratio $T_A(\text{H I})/T_A^*(\text{CO})/\eta > 5$. There is therefore reason to think that the molecular gas is distributed as ubiquitously as the H I in the inner Galaxy. Furthermore, it seems reasonable to utilize the distribution and kinematic molds derived from the more easily observed H I in the interpretation of the molecular data, and, conversely, to refine these models using the higher-resolution and less confused molecular data.

V. THE LATITUDE-VELOCITY ARRANGEMENT OF THE INNER-GALAXY CO EMISSION

In Figures 8–12 we show the latitude-velocity arrangement of CO emission at longitudes displaced from Sgr A West by $\Delta l = +120'$, $+50'$, $0'$, $-50'$, and $-120'$. These b - v cuts demonstrate the effects of the tilted inner-Galaxy geometry. The projected components of the rotation and expansion functions change rapidly with l in b - v cuts; because of this, they can be profitably exploited using the high-angular-resolution molecular observations.

We note several respects in which the tilted-disk distribution satisfies the observed emission patterns shown in Figures 8–12.

1. The tilt in the plane of the sky, given by α , causes emission at both positive and negative velocities to appear at positive longitude and negative latitude and vice versa. Such behavior is clearly present in all the Figures 8–12.

2. The inclination angle i causes positive velocities to appear at higher latitudes than do negative velocities. Below the apparent major axis of the disk expansion velocities are perceived as negative, and above, as positive. This characteristic signature of the model is especially apparent in Figures 10 and 11. At large $|\Delta l|$ the disk signature is expected to be quite asymmetrical about $\Delta b = 0'$ (see Fig. 1). Our data at $|\Delta l| = \pm 120'$ are not sufficiently extensive in latitude to reveal the complete disk signature.

3. Even features with large and obvious noncircular motions should show velocity gradients dv/dl which reflect the presence of rotation. As is clearly the case in Figures 8–12 and also in Figure 2, all high-velocity emission shows the velocity increasing with longitude.

These direct and very general consequences of the model spatial and kinematic distribution obviously play a dominant role in determining the appearance of the observed emission patterns. These patterns would not be expected for a gas distribution confined to the equatorial plane and undergoing circular rotation.

As is the case with many apparently isolated H I features discussed in Paper I, we believe that many of the inner-Galaxy CO features are subsumed by the tilted-disk model. Because the observations conform in general with the predictions inherent in a model incorporating a ubiquitous gas distribution, we believe the molecular distribution may be quite smooth throughout the disk. These conclusions are reinforced by the appearance of a predicted disk signature in

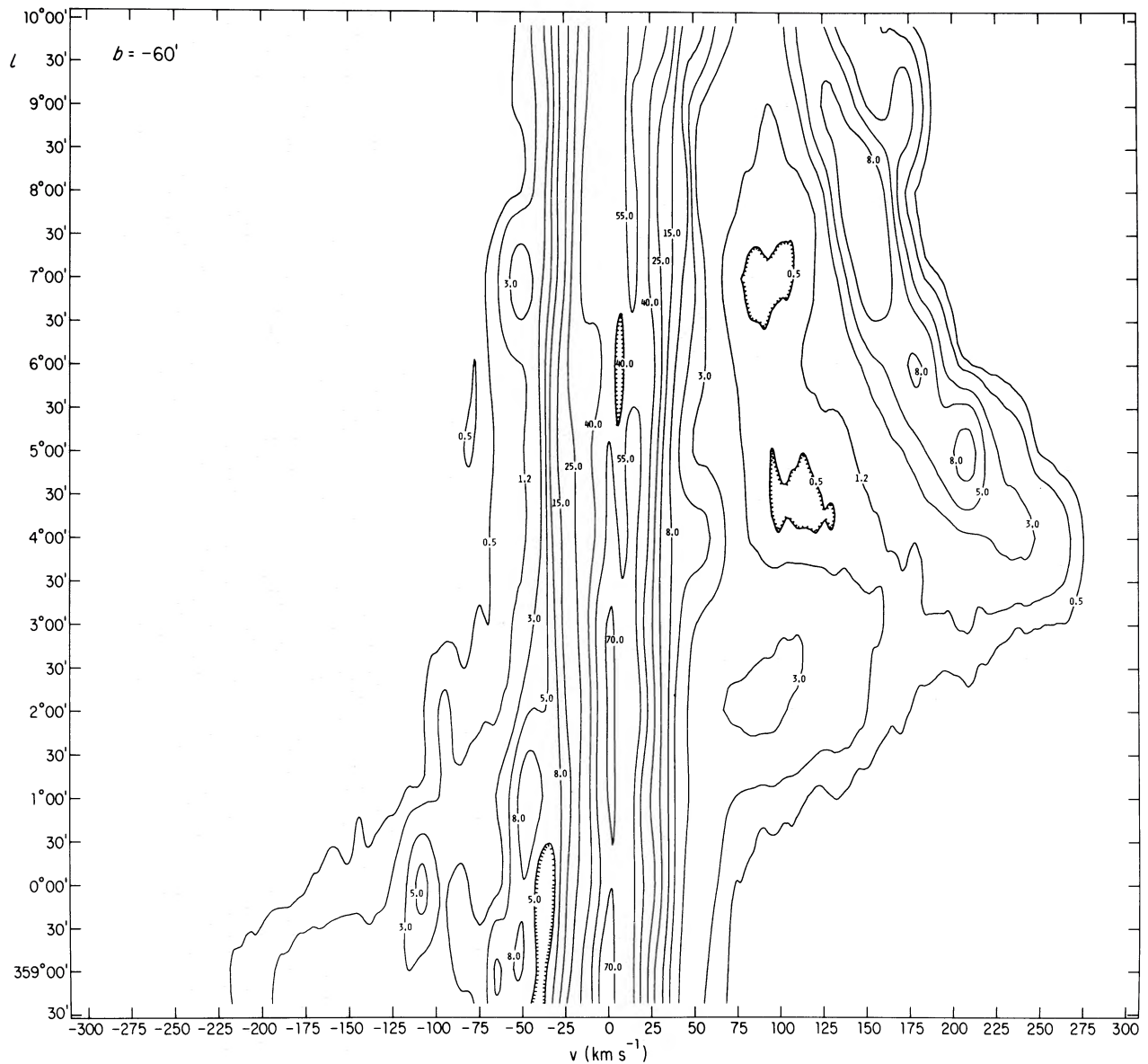


FIG. 5.—Longitude-velocity arrangement of H I emission at $b = -60'$ as observed with 1° beam spacings and 10 km s^{-1} velocity resolution (from the H I material described in Paper I). Contours are drawn at levels $T_A = 0.5, 1.2, 3, 5, 8, 15, 25, 40, \dots$, K. Detectable CO emission appears at the positions and velocities of H I features whenever the antenna temperature at 21 cm exceeds ~ 5 K.

each of the available CO position-velocity cuts through the inner Galaxy and by the existence of counterparts to the CO features in the H I material, which, having been more extensively observed, provides evidence with a more direct bearing on the tilted disk and its parameters.

Figures 8–12 also illustrate several features to which the model has not been extended, including emission which is probably due to the 135 km s^{-1} expanding arm feature in Figure 8. This feature has a patchy distribution in CO, appearing only at $\Delta l = -50'$

(perhaps) and at $+120'$. We note that its emission at $\Delta l = +120'$, like that of the 3 kpc arm and of the Galaxy at large, is approximately symmetrical about the plane $b = -3'$ (the latitude of Sgr A West). On the other hand, the Sgr B2 molecular cloud complex, which dominates the $\Delta l = +50'$ cut (Fig. 9) between $v \approx 25$ and 125 km s^{-1} , has a latitude distribution essentially identical to that of the 165 km s^{-1} expanding feature as it is observed at that longitude. The kinematics of Sgr B2 are certainly aberrant; that this source partakes of the general tilt of the inner-Galaxy

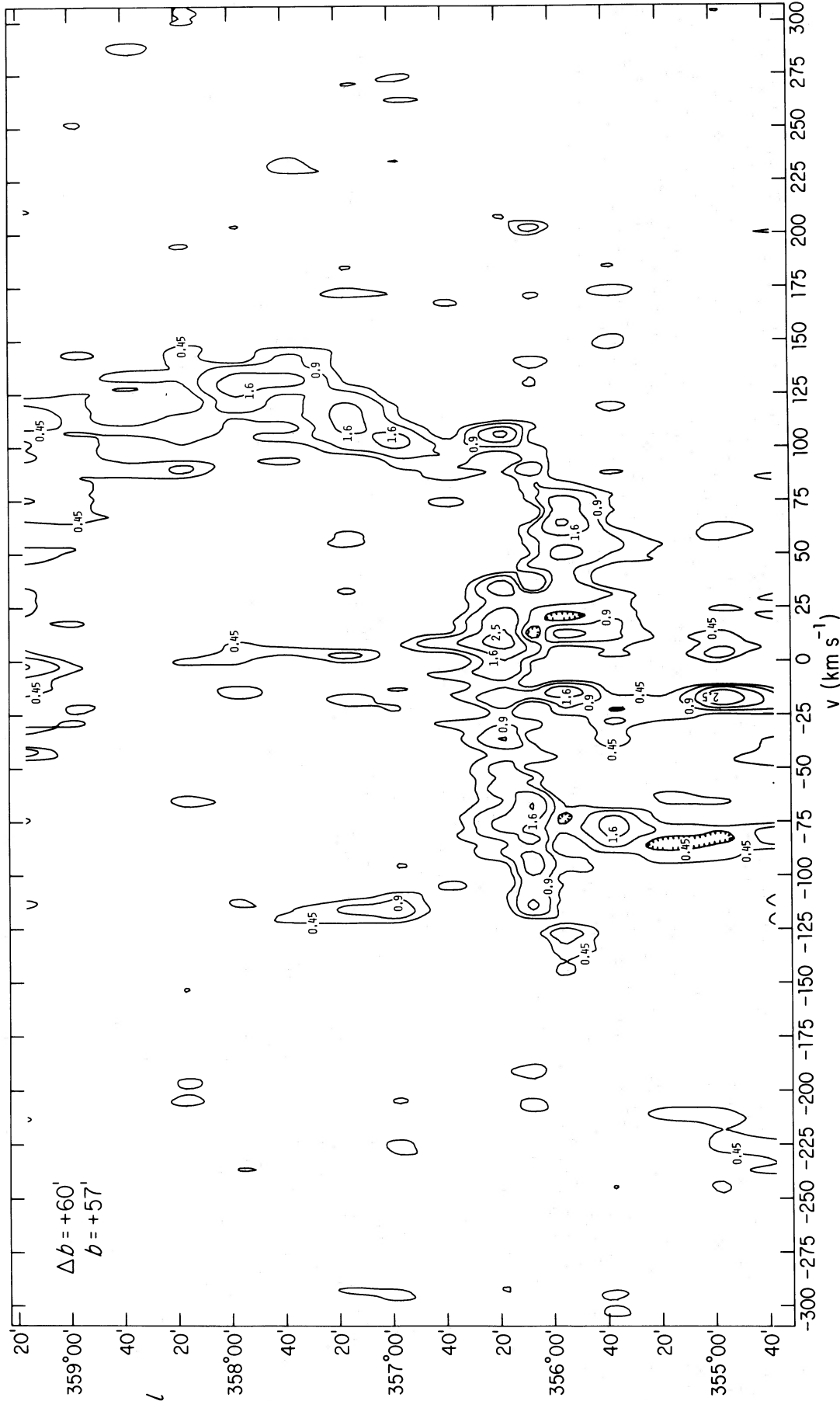


Fig. 6a.—Longitude-velocity arrangement of CO emission at $\Delta b = 60'$ as observed with $20'$ beam spacings and 5 km s^{-1} velocity resolution

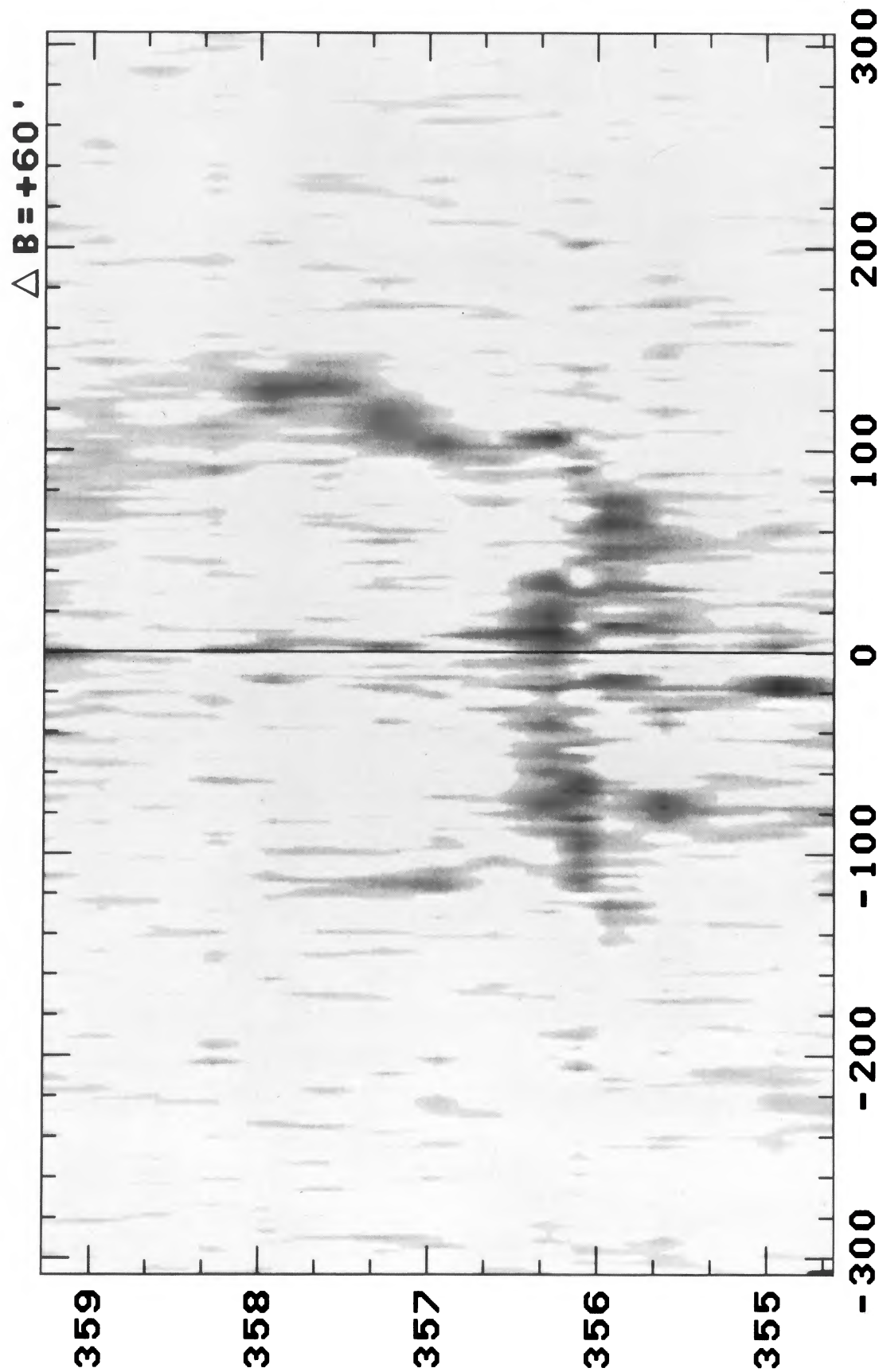


FIG. 6b.—Gray-scale representation of the longitude-velocity arrangement of CO emission at $\Delta b = 60'$, as in Fig. 6a

distribution indicates that it may be possible to fit even this cloud complex within the larger framework described here.

Figure 10 shows that the Sgr A molecular complex has a large velocity gradient dv/db . Such a gradient is reproducible by a tilted model incorporating both rotation and expansion because of the change of sign of the projected expansion motion which occurs as the line of sight crosses the apparent major axis of the disk. (Similarly, negative- and positive-velocity portions of the overall emission patterns generally are separated in latitude.) The concentration of high CO emission intensities to the complex is, of course, not reproduced by the model gas distribution, which is not dependent on ϖ_z . If the model did incorporate a density concentration, however, the resulting emission pattern would show a dv/db gradient similar to the one observed. Although such a central concentration would be quite plausible, the nonzero velocity of the centroid of the complex at $\Delta l = 0'$ would remain a problem in the context of the model. The Sgr A molecular complex covers the positive-velocity interval 25–60 km s⁻¹, despite the fact that it occurs at the longitude of the 2 μ m radiation peak conventionally taken as the longitude of the dynamical center of the Galaxy. Oort (1977) suggests that this velocity shift should be attributed to localized ejection phenomena.

It is worthwhile considering unconventional suggestions regarding the velocity asymmetries at $\Delta l = 0'$. Thus the kinematic characteristics of the Sgr A complex are consistent with a location at a position beyond the midplane of an expanding disk. Alternatively, they are consistent with a situation in which the center of the tilted disk is located at $\Delta l < 0'$. There is some additional evidence of this shift. The two branches of the observed molecular ring (see Fig. 2) cross the $\Delta l = 0'$ plane with different velocities, which average to +15 km s⁻¹. The two corresponding branches which follow from the synthesis (see Fig. 3) are symmetric in velocity in the direction of the center of the disk. No axisymmetric alteration of either the kinematic or the spatial parameters of the model can account for the observed shift. The most straightforward modification of the model which would account for the observed lack of symmetry with respect to $v = 0$ km s⁻¹, $\Delta l = 0'$ involves a displacement of its kinematic center by some 10' to negative longitudes. In this context we note that the molecular emission which does show a strong rotation component is directly observed to cross zero velocity at $l = -10'$ (Liszt *et al.* 1977), where the average velocity of the expanding molecular features is closer to 0 km s⁻¹. Although the continuum source Sgr A West is indeed unique in our Galaxy in a variety of respects (again, see the review of Oort 1977), it is not so clearly distinguished in the molecular observations from which kinematic patterns of the innermost material are most directly derived. Thus, for example, the position of the 2 μ m intensity peak in Sgr A West is noticeable in CO only to the extent that molecular emission is rather weak there (Liszt, Sanders, and Burton 1975). Recently, Rieke, Telesco, and Harper

(1977) have argued that the appearance of the near-infrared intensity distribution is seriously modulated by absorption in intervening molecular clouds, a conclusion supported by the submillimeter work of Hildebrand *et al.* (1978). It is at least worth considering that the gaseous mass distribution may not be exactly concentric with the apparent light distribution, as had previously been assumed to be the case. We argue in this series of papers that the inner-Galaxy gas kinematics are regular and predictable on even small angular scales. In view of these points, we believe that an unorthodox placement of the kinematic center of the Galaxy must not be rejected without good reason. Detailed CO observations of the inner half-degree of the Galaxy would provide the best material with which to confront this question.

VI. PHYSICAL PROPERTIES OF THE MOLECULAR GAS IN THE INNER GALAXY

The intensity of the molecular gas features in the inner Galaxy, typically 1–2 K, is quite similar to that observed from equally distant portions of the general galactic layer (Burton and Gordon 1978). However, the emission discussed here is unique in several important respects. In particular, CO emission from the inner Galaxy has the following characteristics:

1. It has a much smoother spatial distribution, with little of the patchy appearance that leads one to deduce a typical cloud size 5–30 pc characterizing the galactic layer.

2. It appears concentrated in one or two broad but well-defined features at any given position, with typical widths 20–40 km s⁻¹. Such broad features are observed outside the galactic nucleus only toward such complex regions as W51 A (Scoville and Solomon 1974).

3. It is extremely strong relative to the H I observed at similar positions. The carbon monoxide intensity is only a factor ~ 5 below that of H I; in the Galaxy at large, the intensities differ typically by much more than an order of magnitude.

4. It has kinematics which are essentially identical to those of H I. Whenever the antenna temperature at 21 cm exceeds about 5 K, CO emission is present at a level greater than ~ 1 K (T_A^*/η).

The smooth appearance of the inner-Galaxy molecular emission and its similarity to H I argue for a ubiquitous molecular distribution within the tilted disk. The very large velocity widths of the observed molecular features are understandable only in terms of velocity projection effects, which in turn cannot be effective except in a very generally distributed gas.

Using the model parameters discussed in Paper I and in § II, we have for the masses of H I and H₂ within the tilted disk distribution

$$\begin{aligned} M_{\text{H I}} &= 4 \times 10^7 [n_{\text{H I}}(0)/1 \text{ cm}^{-3}] M_{\odot}, \\ M_{\text{H}_2} &= 8 \times 10^7 [n_{\text{H}_2}(0)/1 \text{ cm}^{-3}] M_{\odot}, \end{aligned} \quad (5)$$

if mean densities in the midplane are denoted by $n(0)$. For H I, $n_{\text{H I}}(0) = 0.33 \text{ cm}^{-3}$ reproduces the observed line intensities if the spin or kinetic temperatures are

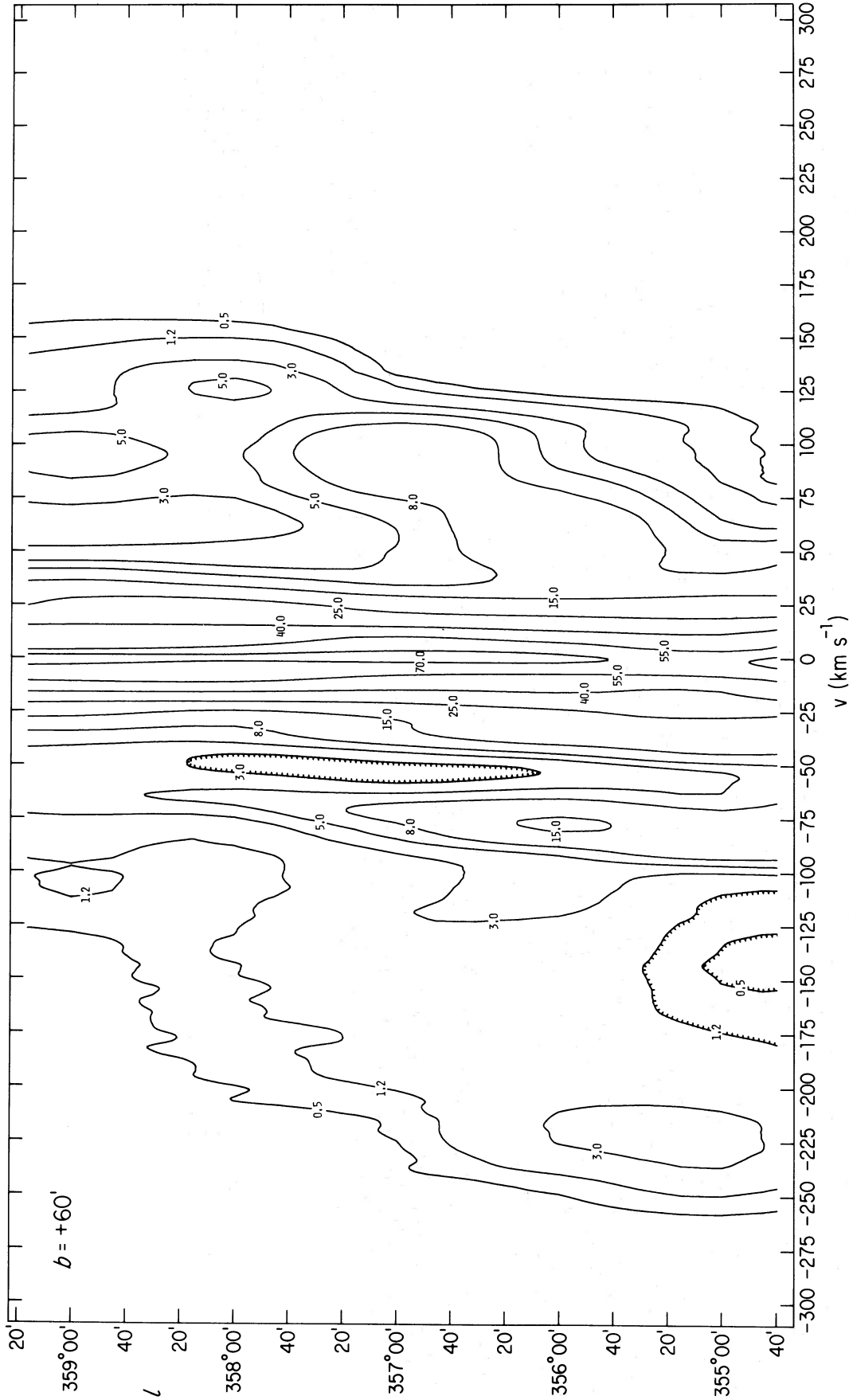


FIG. 7.—Longitude-velocity arrangement of H I emission at $b = 60'$, with parameters as in Fig. 5. Note the coincidence of the CO ridges in Figs. 6a-6b with those shown here. Differences in appearance between CO and H I emission are more likely caused by the low contrast in the CO maps than by any profound difference in their spatial or kinematic distribution.

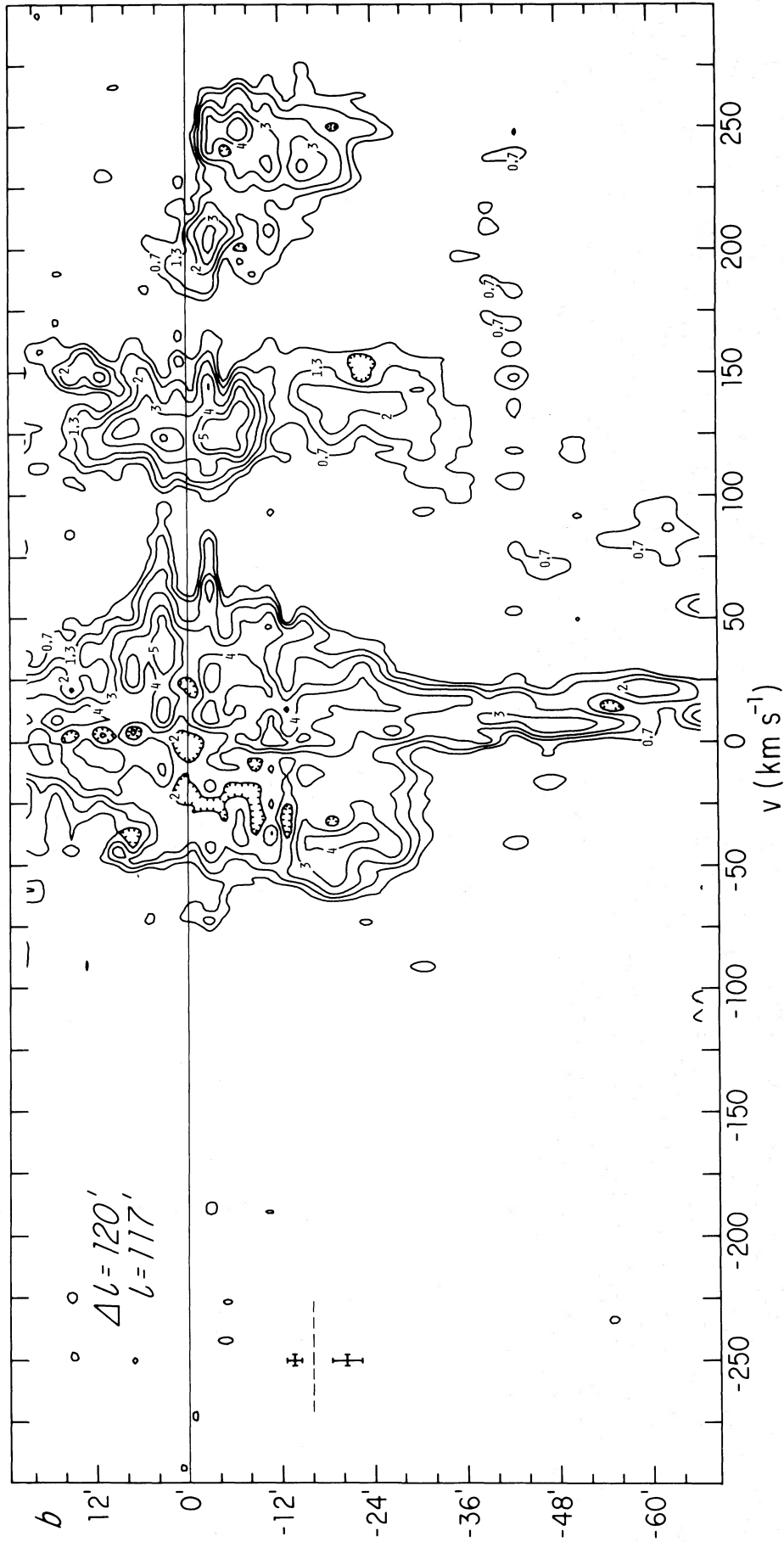


FIG. 8a.—Latitude-velocity arrangement of CO emission at $\Delta l = +120'$. The molecular ring feature has disappeared, and emission at $v \lesssim 200 \text{ km s}^{-1}$ lies below $b = 0'$. The feature at $v \approx 125\text{--}150 \text{ km s}^{-1}$ is more symmetrically placed about the galactic equator and cannot be traced between $-50' < l < 120'$.

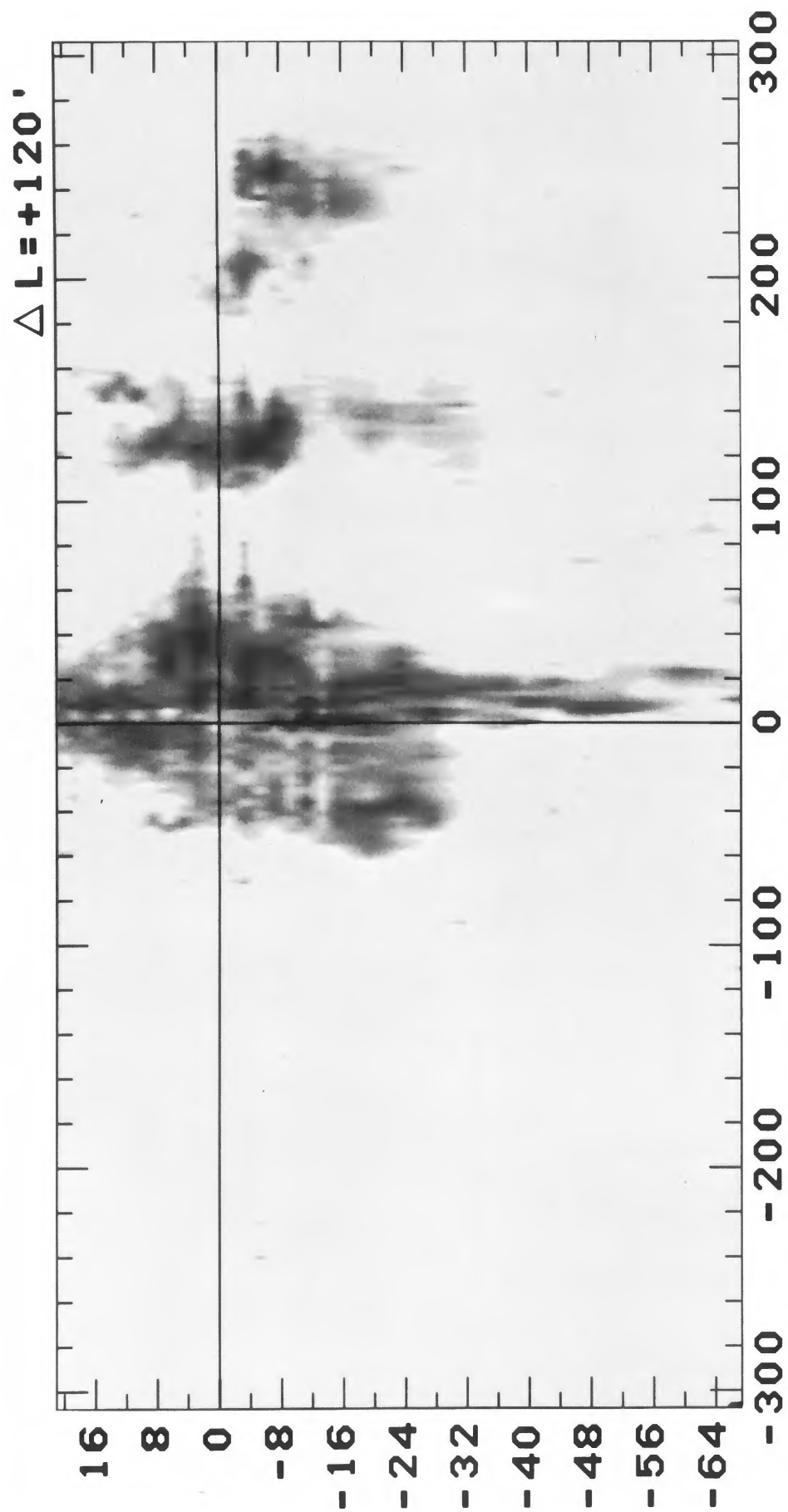


FIG. 8b.—Gray-scale representation of the latitude-velocity arrangement of CO emission at $\Delta l = +120'$, as in Fig. 8a

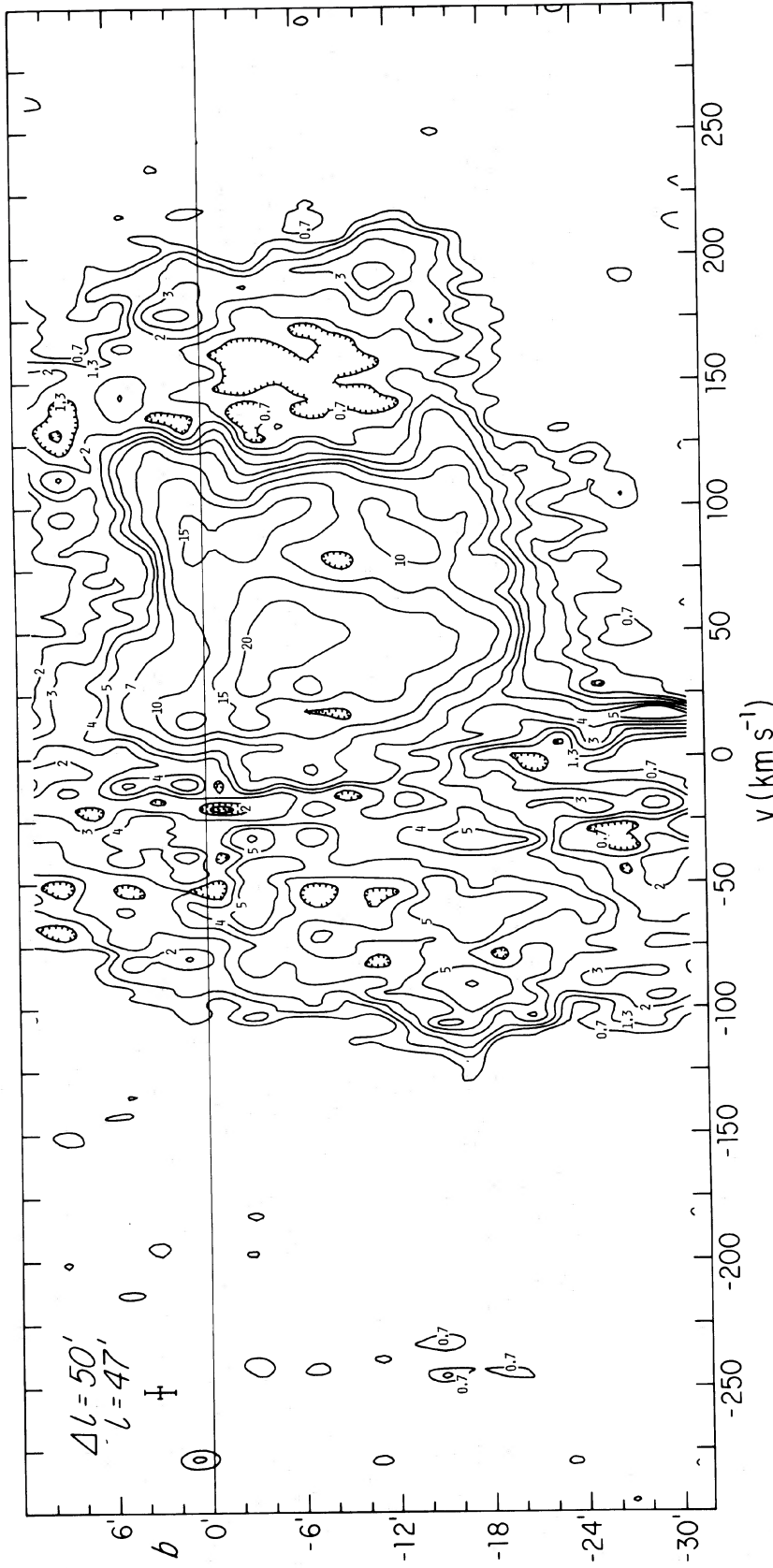


Fig. 9a.—Latitude-velocity arrangement of CO emission at $\Delta l = +50'$, as observed with $2'$ beam spacings and 5 km s^{-1} velocity resolution. The high-velocity gas here is predominantly below $b = 0'$, a characteristic shared by the Sgr B2 clouds at $0 \text{ km s}^{-1} \lesssim v \lesssim 125 \text{ km s}^{-1}$.

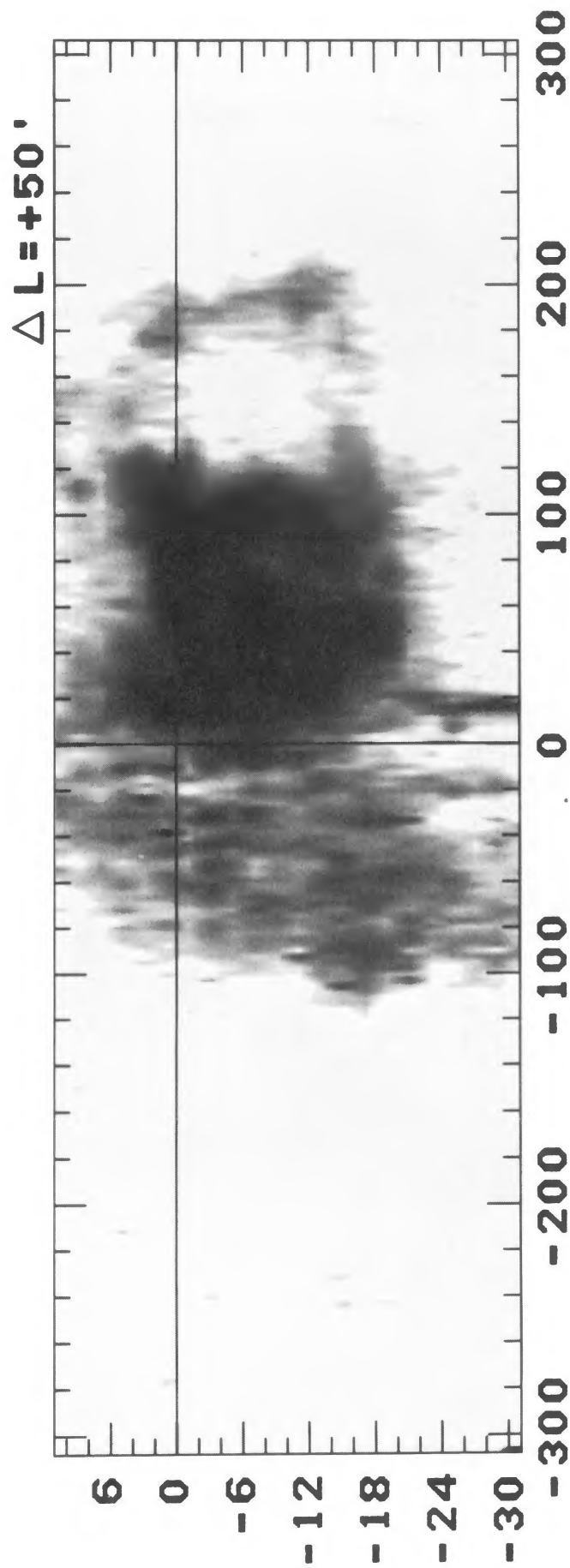


FIG. 9b.—Gray-scale representation of the latitude-velocity arrangement of CO emission at $\Delta l = +50'$, as in Fig. 9a

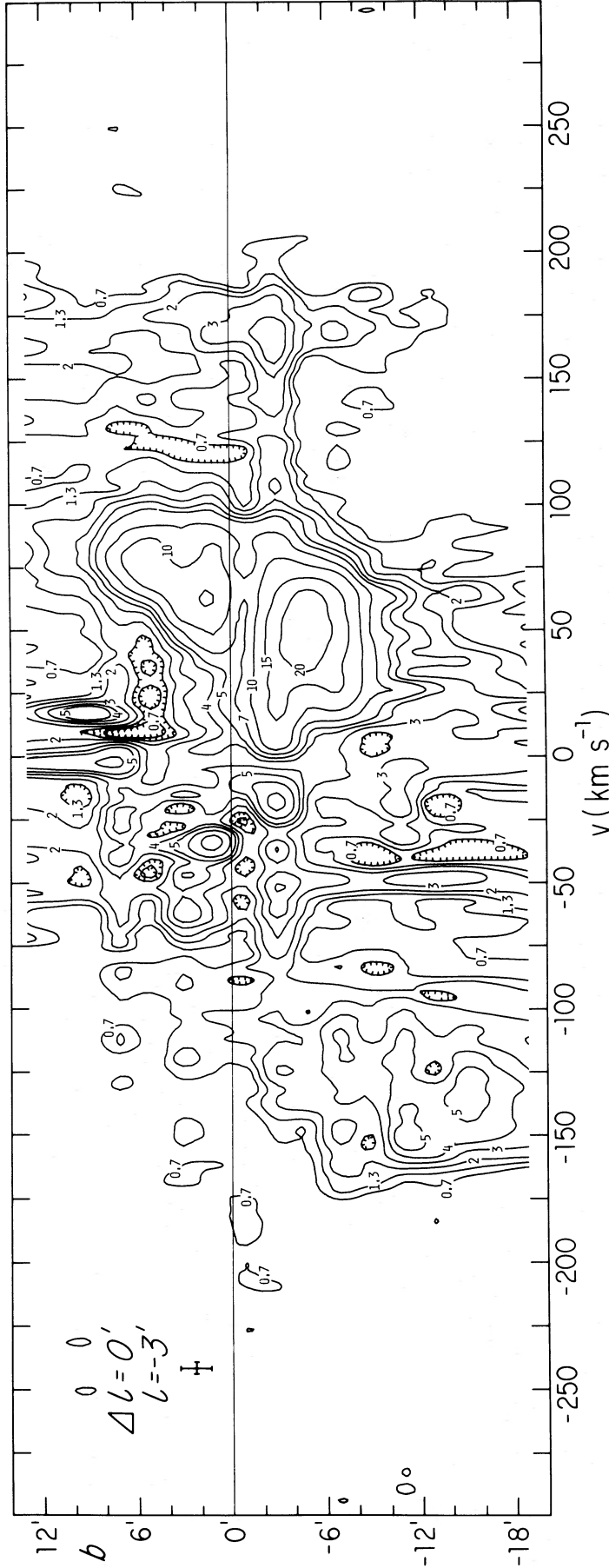


FIG. 10a.—Latitude-velocity arrangement of CO emission at $\Delta l = 0'$, as observed with $2'$ beam spacings and 5 km s^{-1} velocity resolution. The expanding molecular features are symmetrically displaced about $\Delta b = 0'$ but not about $v = 0 \text{ km s}^{-1}$. The Sgr A clouds at $0 \text{ km s}^{-1} \lesssim v \lesssim 100 \text{ km s}^{-1}$ have an appreciable velocity gradient dv/db ; as discussed in § V, such behavior would follow if our model included a central mass concentration.

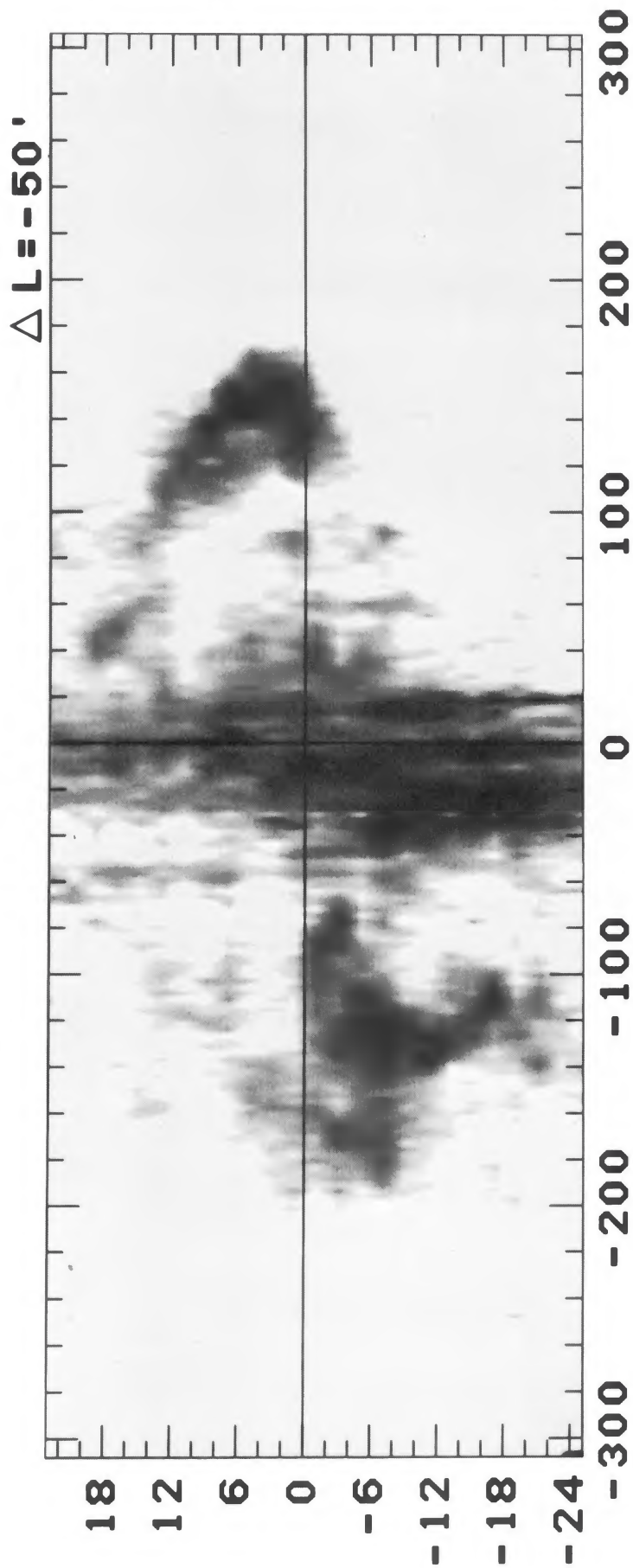


FIG. 11b.—Gray-scale representation of the latitude-velocity arrangement of CO emission at $\Delta l = -50'$, as in Fig. 11a

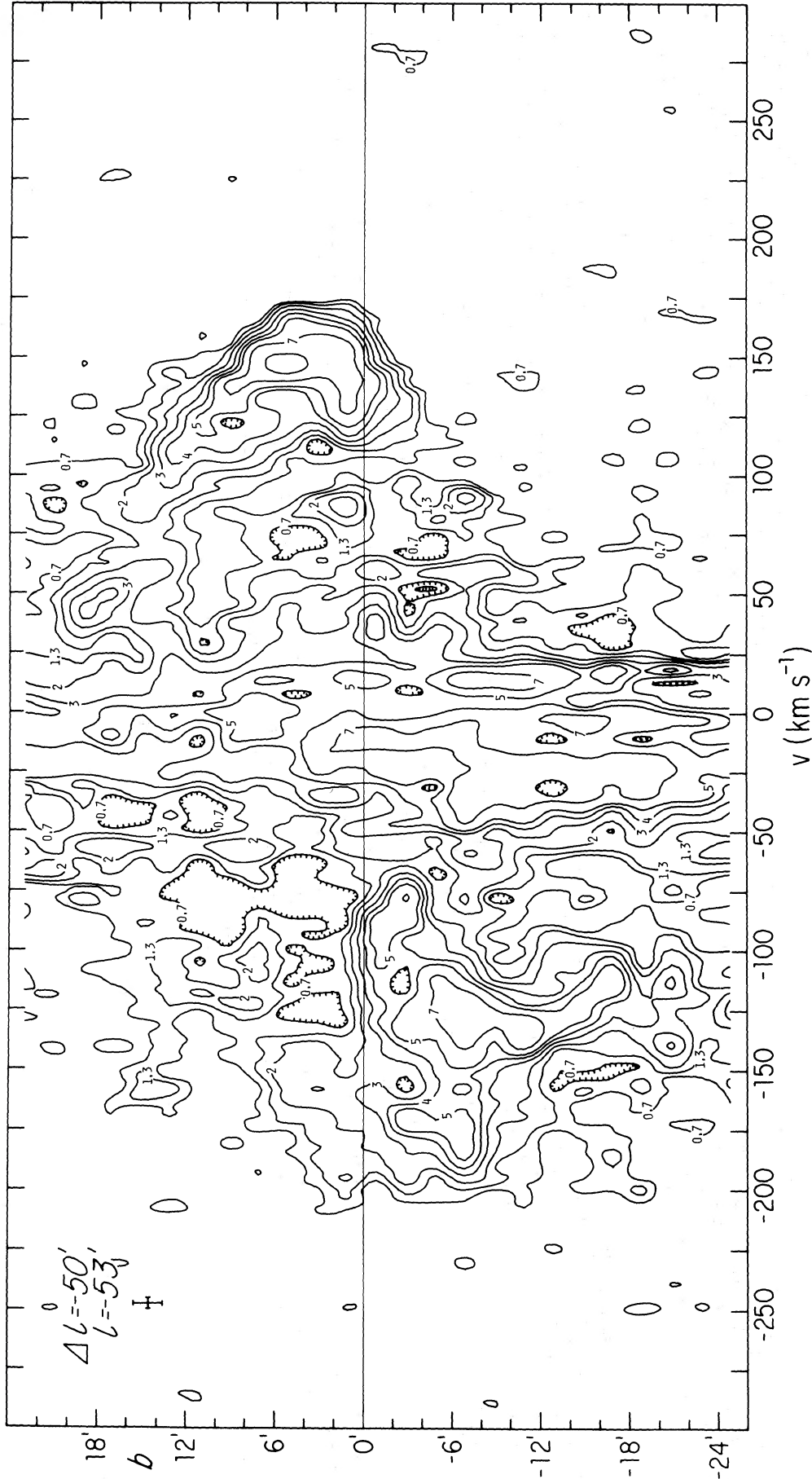


FIG. 11a.—Latitude-velocity arrangement of CO emission at $\Delta l = -50'$, as observed with $2'$ beam spacings and 5 km s^{-1} velocity resolution. Note that the emission pattern of the high-velocity gas occurs closer to $b \approx 0'$ than in Fig. 12 but with the same characteristic separation in latitude of positive and negative velocities.

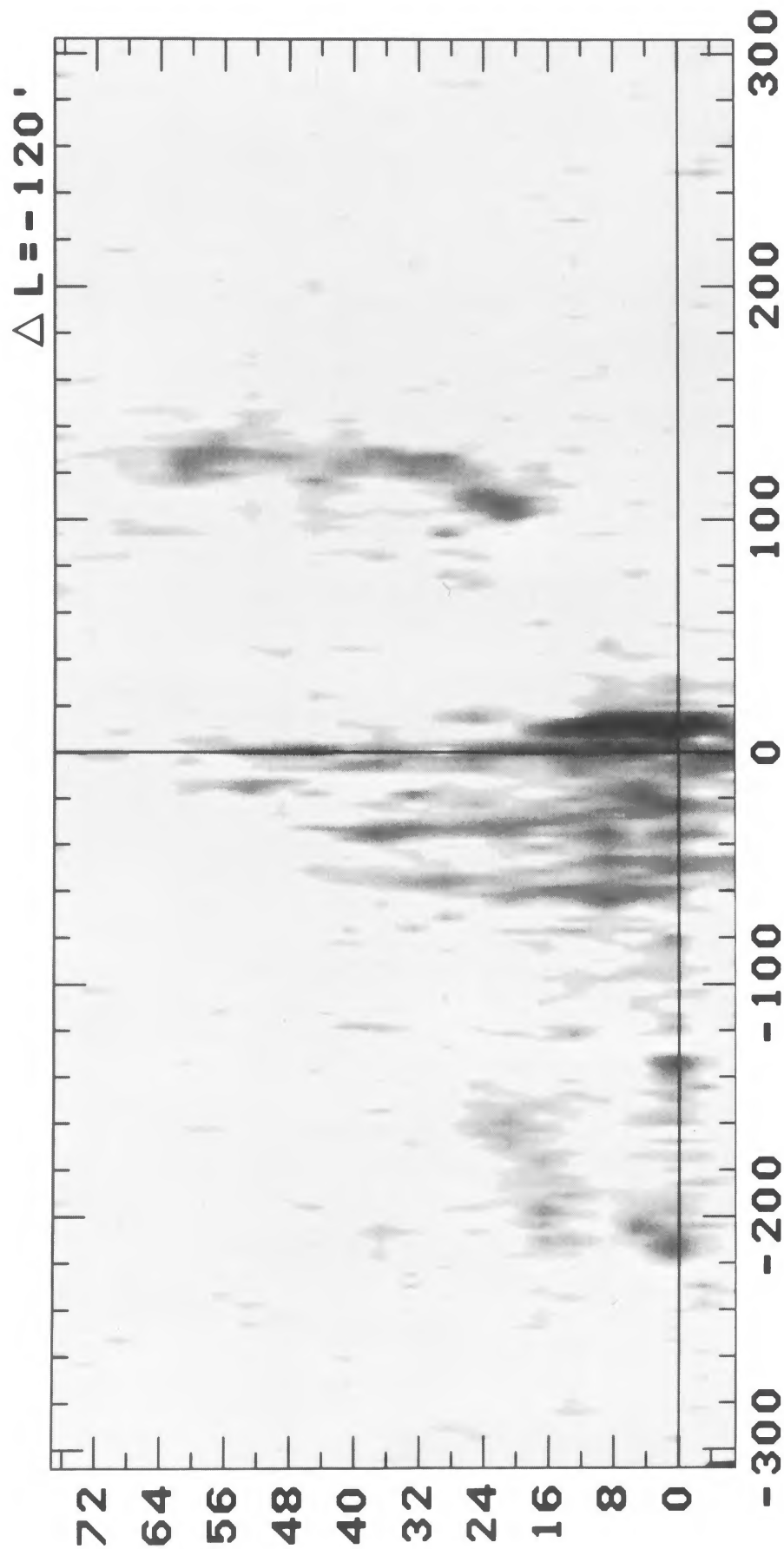


Fig. 12*b*.—Gray-scale representation of the latitude-velocity arrangement of CO emission at $\Delta l = -120'$, as in Fig. 12*a*

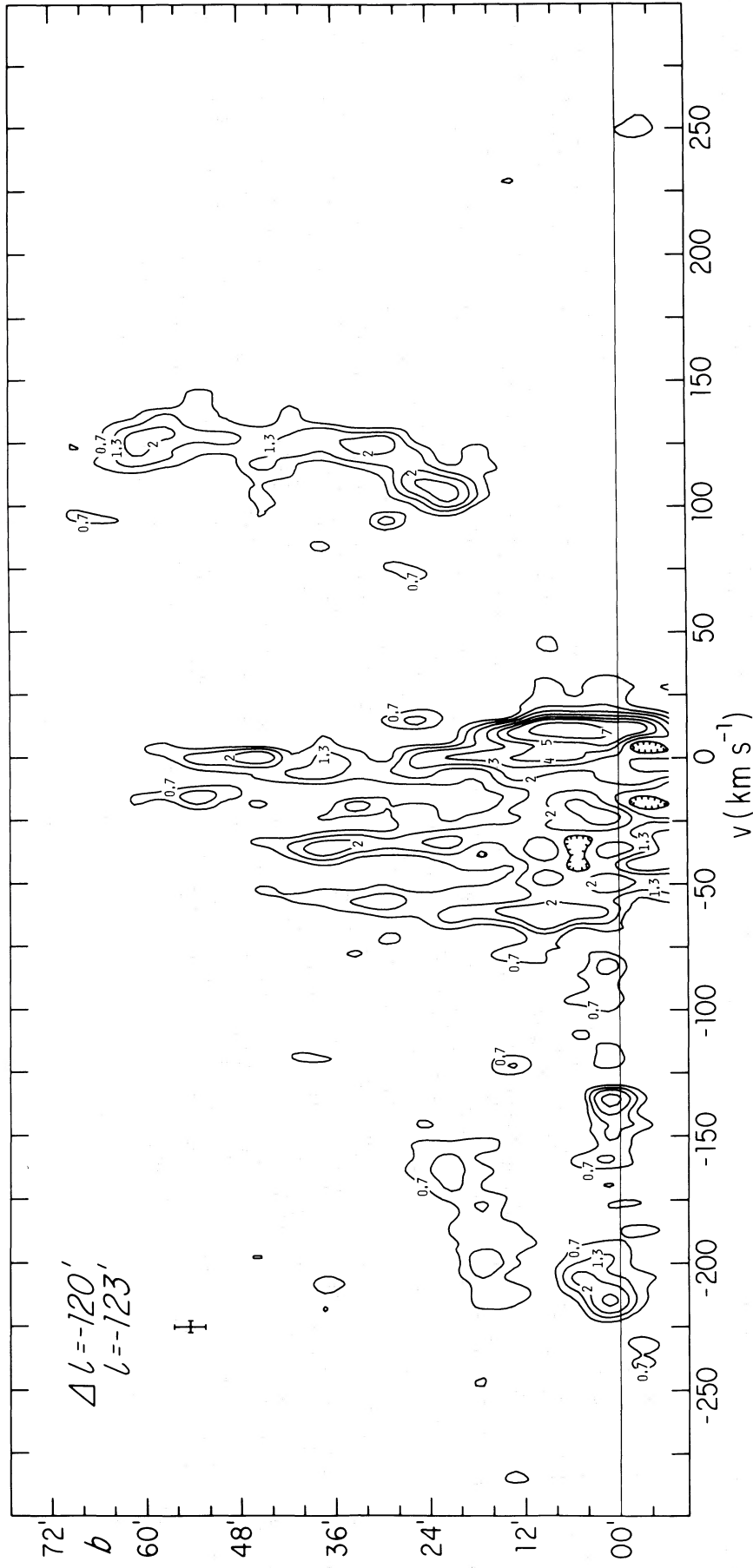


FIG. 12a.—Latitude-velocity arrangement of CO emission at $\Delta l = -120'$, as observed with $4'$ beam spacings and 5 km s^{-1} velocity resolution. Emission from high-velocity gas occurs at $b \gtrsim 0'$, and positive velocities occur at more positive latitudes than do negative velocities. These characteristics are indicative of the tilts of the inner-Galaxy gas distribution, as discussed in § V of the text.

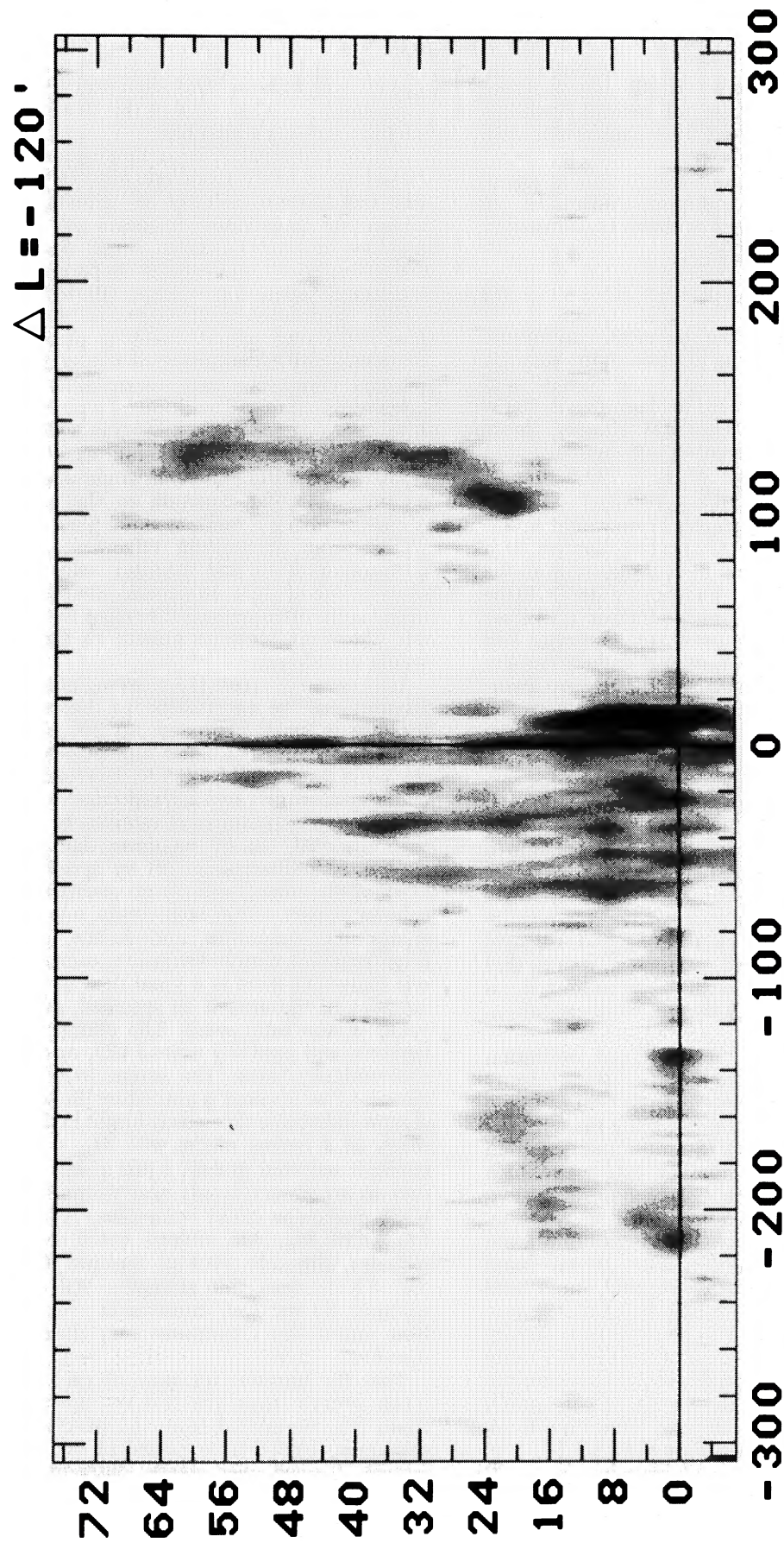


FIG. 12b.—Gray-scale representation of the latitude-velocity arrangement of CO emission at $\Delta l = -120'$, as in Fig. 12a

high ($T_{\text{spin}} = 120$ K). Changes in the assumed spin temperature can only increase the neutral hydrogen density because the observed H I emission is well modeled by an optically thin gas.

In the simplest case of a uniform molecular gas in which carbon monoxide rotation transitions are excited only by collisions with ambient H_2 molecules, the observed intensities imply

$$n_{\text{H}_2} T_k \gtrsim 1-2 \times 10^4 \text{ cm}^{-3} \text{ K} \quad (6)$$

as a direct consequence of statistical equilibrium calculations of population distribution in the rotation ladder (using the rate constants of Green and Thaddeus 1976). If the kinetic temperature is below ~ 15 K, the required density rises sharply (more rapidly than T_k^{-1}) as conditions of line thermalization are more nearly demanded. If $T_k = 120$ K, $n_{\text{H}_2} \approx 100-200 \text{ cm}^{-3}$ and $M_{\text{H}_2} \approx 5-10 \times 10^9 M_\odot$ is obtained for the disk mass. This is higher than would be inferred from the observed CO spectral features. If a single emission line is present at every position in the disk with a width 30 km s^{-1} and optical depth 3 (the observed emission must be optically thick if low values for the excitation temperatures are assumed) and typical intensity, one infers a typical column density $N_{\text{CO}} = 2 \times 10^{17} \text{ cm}^{-2}$. Even for a low relative abundance of carbon monoxide with respect to hydrogen $[\text{CO}]/[\text{H}_2] = 3 \times 10^{-5}$, the integral of N_{H_2} over the projected disk area is only $M_{\text{H}_2} \approx 10^9 M_\odot$. The disparity between the two mass estimates arises for two reasons. First, the path length over which a typical feature is formed, 200–300 pc, is much less than the distance over which a typical line of sight remains in regions of the disk bearing significant density. Over most of these lines of sight, the apparent velocity gradients are large and consequently the line opacity and the intensity are much reduced. Second, we have not taken care in the second estimate to ensure that the inferred mean density is in fact large enough, at an optical depth of 3, to provide the necessary excitation, which in fact it is not.

Arguments based only on collisional excitation usually overestimate the inferred density. If the opacity is greater than unity, the line radiation field can be a significant source of excitation, lowering the required density of collision partners (Scoville and Solomon 1974; Leung and Liszt 1976). The extent to which photon trapping is effective will be limited by two circumstances. First, the gas must still be relatively warm, because the opacity required to reach a given excitation condition increases sharply as one nears conditions of line thermalization. Second, the optical depth required should in principle be available over 200–300 pc path lengths. As the assumed density decreases over a fixed path length, the required opacity and abundance ratio $[\text{CO}]/[\text{H}_2]$ will rise: because the CO abundance is bounded, there must be a minimum density consistent with the observed intensities. If we require only the very mild condition $[\text{CO}]/[\text{H}_2] = 3 \times 10^{-4}$, opacities $\tau \approx 50$ are available when $n_{\text{H}_2} = 20 \text{ cm}^{-3}$. In the work of either Scoville and Solomon (1974)

or Leung and Liszt (1976), such opacities are required, even at $T_k \approx 100$ K, so that this density is about the smallest that is permissible.

Another alternative is to clump the molecular gas. It follows directly from the observations, however, that these clumps will not be “clouds,” as these are commonly understood to occur in the molecular annulus of the Galaxy at large. Such clouds are characterized by diameters 5–30 pc and by a typical intercloud separation ~ 1 kpc (Burton and Gordon 1978). The total area of the disk is 7 kpc^2 , and only a few dozen such clouds could be present within the boundaries of the midplane of the model. In fact, the relevant clump sizes and separations could not be large even compared with our 2.9 pc beam diameter. If one constructed a distribution in which individually detectable clumps had separations which were not small compared to 200 pc, it would not be possible to confine molecular emission to the ridges that are observed. Given a random cloud placement, emission would occur at random velocities within a range corresponding to the external velocities perceived along a line of sight. In general, emission would then occur more often outside the ridges than within them, and the clear patterns present in the observations would not appear.

In order to re-create the observed patterns, clumped models must be constrained so that the interclump distance is small compared to 200 pc and so that individual clumps produce emission which is below our noise threshold of ~ 0.5 K. The formal parameters of clumped models are easily specified. (1) By requiring that the aggregate emission received be comparable to that observed, (2) by requiring that the individual clumps be undetectable, (3) by specifying the total mass of the model, and (4) by specifying a minimum column density within each clump, one can derive the clump size, separation, and density, as well as the brightness temperature intrinsic to each clump. Indeed, one finds that there is a great deal of latitude in the qualities of the models so specified, even at a single value of the total mass. The clumps may be hot, tenuous, and optically thin in CO, or colder, denser, and optically thick. The extent to which the total mass may be lowered is limited by the tendency of the clumps to become excessively bright in the lowest-mass cases. In a typical model with $M_{\text{H}_2} = 10^8 M_\odot$, each clump is required to emit a line of intensity 30–50 K, such as are observed only near strong heat sources in giant molecular cloud complexes. Alternatively, for $M_{\text{H}_2} = 10^9 M_\odot$, the clumps could resemble small globules, with radii ~ 0.4 pc, densities 500–1000 cm^{-3} , and 5 K intrinsic line strengths. All clump models specified by the four constraints enumerated above have interclump separations very close to the beam diameter, ~ 3 pc.

That the intrinsic intensity of each clump is not much greater than the 3–4 K observed intensities could also be argued from the observations. If one compared the spectra expected of two equally broad features formed over greatly different path lengths, one would present more clumps to the beam. Unless

the excitation temperature in the clumps were close to the minimum value deduced from the observations, the two features would also differ in intensity in a predictable manner. A similar consideration arises in models which are uniform and in which the excitation temperatures are sensitive to the line opacities, but no such strong variations are apparent in the data. In any case, we cannot produce a consistent model in which the total mass of gas is appreciably below $10^9 M_{\odot}$.

Molecular observations currently available are insufficient for deducing either the actual mass of gas in the disk or the mechanism of line production, but several observational constraints are possible. Longer integration times should lead the CO emission to resemble even more closely that of H I and to appear smoothly outside the prominent emission ridges. Observations of ^{13}CO should show intensity variations according to the path lengths corresponding to the various features, if the molecular distribution is ubiquitous and the ^{13}CO lines are of sufficiently low opacity. Last, observations with differing beam sizes might indicate the beam-filling factors of clumped models.

Although the amount of gas in the inner-Galaxy disk could be quite large, it is not necessarily very different from the mass derived from analysis of the negative-longitude, negative-velocity portion of the rotating nuclear disk signature in H I. As discussed by Oort (1977), such a procedure leads to a total mass $\sim 2 \times 10^{10} M_{\odot}$ interior to $\varpi = 1$ kpc. If 4% of this mass is in gaseous form, as elsewhere in the Galaxy (Gordon and Burton 1976), it would correspond to a mean density $n_{\text{H}_2} = 25 \text{ cm}^{-3}$ in our model. Alternatively, the large observed CO/H I intensity ratios could indicate that the inner Galaxy is exceptionally rich in gaseous matter, and even higher molecular densities would lead to total gaseous masses similar to those that have already been derived. The strongest constraints on the inner-Galaxy distribution will arise from a more thorough discussion of the relationship of this material to the general galactic layer. In Paper I it was shown that the available large-scale H I observations are consistent with the present model, even though we have made no attempt to join smoothly the kinematics of material within and beyond the disk boundaries (there are in fact "bulges" in the observed H I terminal velocities at positions where certain l - v maps "cross" the hypothetical disk boundaries). However, purely circular motion undoubtedly obtains over much of the Galaxy and may dictate a value for the interior mass. Because our model contains a pervasive expansion component, circular velocity is not related in an obvious fashion

to the gravitational potential and so cannot be used to specify the total mass distribution. Although it is unlikely that a tilted gas distribution could persist without reflecting in some way the dynamics of the total mass distribution, the interaction remains to be specified. It is important to note that our Galaxy would not be unique in having an inner distribution which did not coincide with the mean plane of the rest of the matter. Such a situation is now known to occur in M31 (Light, Danielson, and Schwarzschild 1974) and in other galaxies cited in Paper I.

Because we infer a density $n_{\text{H I}}$ and extent z for the disk which are quite similar to those found elsewhere in the Galaxy, it follows that the proposed H I surface density deficiency at $\varpi < 1.5$ kpc (e.g., Burton 1976) may need reconsideration, utilizing data away from the galactic equator in addition to the $b = 0^{\circ}$ material. If the abundance of H I is normal, it follows that H_2 is actually overabundant in this region. Between galactocentric radii 4–8 kpc, the mean (volume-averaged) density is in the range $n_{\text{H}_2} = 1\text{--}5 \text{ cm}^{-3}$ (Gordon and Burton 1976). Interior to 1.5 kpc, however, it is unlikely that the mean molecular density is less than about 20 cm^{-3} . This amount of material, if spread uniformly in the galactic layer out to 4 kpc, would produce a mean density 3 cm^{-3} , and in a gross sense there is perhaps no deficiency of molecular gas in the inner 8 kpc of the Galaxy. In order to determine the nature of the gas distribution within the annulus $\varpi = 2\text{--}4$ kpc, observations out of the galactic equator are certainly required.

VII. SUMMARY

1. The tilted-disk model of the inner-Galaxy gas distribution used in Paper I reproduces the expanding molecular features observed in the galactic equator without invoking the existence of material bodies or kinematic perturbations.
2. The kinematics and distribution of H I and CO in the inner Galaxy are essentially identical.
3. The kinematics of the inner-Galaxy molecular gas are extremely regular on large and small angular scales, and exhibit the predictions of the tilted-disk model.
4. Molecular gas is overabundant in the inner Galaxy, relative to either the inner-Galaxy H I or the molecular density in the rest of the Galaxy.
5. The gaseous mass in the inner 1.5 kpc of galactocentric radius is greater than $\sim 1\text{--}2 \times 10^9 M_{\odot}$.
6. The observations suggest consideration of the possibility that the center of kinematic symmetry of the inner-Galaxy gas distribution is displaced from Sgr A West by some $10'$ in longitude.

REFERENCES

- Bania, T. M. 1977, *Ap. J.*, **216**, 381.
 Becklin, E. E., and Neugebauer, G. 1975, *Ap. J. (Letters)*, **200**, L71.
 Burton, W. B. 1976, *Ann. Rev. Astr. Ap.*, **14**, 275.
 Burton, W. B., and Gordon, M. A. 1978, *Astr. Ap.*, **63**, 7.
 Burton, W. B., and Liszt, H. S. 1978, *Ap. J.*, **225**, 815 (Paper I).
 Cohen, R. J., and Davies, R. D. 1976, *M.N.R.A.S.*, **175**, 2.
 Cohen, R. J., and Few, R. W. 1976, *M.N.R.A.S.*, **176**, 495.
 Gordon, M. A., and Burton, W. B. 1976, *Ap. J.*, **208**, 346.

- Green, S., and Thaddeus, P. 1976, *Ap. J.*, **205**, 766.
 Hildebrand, R. H., Whitcomb, S. E., Winston, R., Stiening, R. F., Harper, D. A., and Moseley, S. H. 1978, *Ap. J. (Letters)*, **219**, L101.
 Kaifu, N., Kato, T., and Iguchi, T. 1972, *Nature Phys. Sci.*, **238**, 105.
 Kerr, F. J. 1967, in *Radio Astronomy and the Galactic System*, ed. H. van Waerden (London: Academic Press), p. 239.
 Leung, C. M., and Liszt, H. S. 1976, *Ap. J.*, **208**, 732.
 Light, E. S., Danielson, R. E., and Schwarzschild, M. 1974, *Ap. J.*, **194**, 257.
 Liszt, H. S., Burton, W. B., Sanders, R. H., and Scoville, N. Z. 1977, *Ap. J.*, **213**, 38.
 Liszt, H. S., Sanders, R. H., and Burton, W. B. 1975, *Ap. J.*, **198**, 537.
 Oort, J. H. 1977, *Ann. Rev. Astr. Ap.*, **15**, 295.
 Rieke, G. H., Telesco, C. M., and Harper, D. A. 1977, preprint.
 Rougoor, G. W. 1964, *Bull. Astr. Inst. Netherlands*, **17**, 381.
 Rougoor, G. W., and Oort, J. H. 1960, *Proc. Nat. Acad. Sci.*, **46**, 1.
 Sanders, R. H., and Bania, T. M. 1976, *Ap. J.*, **204**, 341.
 Sanders, R. H., and Lowinger, T. 1972, *A.J.*, **77**, 292.
 Sanders, R. H., and Wrixon, G. T. 1974, *Astr. Ap.*, **33**, 9.
 Sanders, R. H., Wrixon, G. T., and Mebold, U. 1977, *Astr. Ap.*, **61**, 329.
 Scoville, N. Z. 1972, *Ap. J. (Letters)*, **175**, L127.
 Scoville, N. Z., and Solomon, P. M. 1974, *Ap. J. (Letters)*, **187**, L67.
 Scoville, N. Z., Solomon, P. M., and Jefferts, K. B. 1974, *Ap. J. (Letters)*, **187**, L67.
 van der Kruit, P. C. 1970, *Astr. Ap.*, **4**, 462.

W. B. BURTON: Department of Astronomy, University of Minnesota, 116 Church Street Southeast, Minneapolis, MN 55455

H. S. LISZT: National Radio Astronomy Observatory, Edgemont Road, Charlottesville, VA 22901